

Two-dimensional traveling waves arising from planar front interaction in a three-species competition-diffusion system

Lorenzo Contento¹  · Masayasu Mimura² · Makoto Tohma³

Received: 3 July 2015 / Revised: 5 October 2015 / Published online: 17 October 2015
© The JJIAM Publishing Committee and Springer Japan 2015

Abstract From the ecological point of view of competitor-mediated coexistence, we consider a three-species competition-diffusion system which models one exotic competing species W invading the native system of two strongly competing species U and V . Even if W is weaker than the native species, it is found that both competitive exclusion and competitor-mediated coexistence may occur, depending on the growth rate of W . Firstly, we show that there are two different planarly stable traveling waves involving the species (U, V) and (U, V, W) , respectively. Studying the interaction of these waves in one dimension offers insight about whether or not coexistence occurs in two-dimensional domains. However, when planar fronts collide at a certain angle, phenomena which are not immediately reducible to the one-dimensional case can be observed, such as wedge-shaped patterns. In particular, the interaction between a radial and a planar front produces different types of moving patterns which seem to tend to truly two-dimensional traveling waves, such as wedge-, zipper- and biwedge-shaped traveling waves. All these waves arise from the interaction of stable planar fronts and their velocities can be computed by only knowing their asymptotic behaviour. We also show how such waves exist only if the angle between the planar fronts is under a certain critical value.

L. Contento has been supported by Meiji University MIMS Ph.D. Program.

✉ Lorenzo Contento
lorenzo.contento@gmail.com

¹ Graduate School of Advanced Mathematical Sciences, Meiji University, Tokyo 164-8525, Japan

² Meiji Institute for Advanced Study of Mathematical Sciences, Meiji University, Tokyo 164-8525, Japan

³ Department of Economics, Momoyama Gakuin University, Izumi 594-1198, Japan

Keywords Competition-diffusion system · Competitor-mediated coexistence · Wedge-shaped traveling waves · Interaction of planar propagating fronts

Mathematics Subject Classification 35C07 Traveling wave solutions · 35K57 Reaction-diffusion equations · 35Q92 PDEs in connection with biology and other natural sciences

1 Introduction

Understanding of the mechanism behind the rich biodiversity observed in natural ecosystems is an active field of research in mathematical ecology. One possible cause of biodiversity is considered to be *competitor-mediated coexistence*. As a simple example of such phenomenon, take an ecosystem inhabited by three ecological species, two of which are strongly competing native species (say, U and V) and the third is an exotic competing species (say, W). If U and V cannot coexist when W is absent but are able to do so after W invades the ecosystem, we say that competitor-mediated coexistence has occurred. The occurrence of such coexistence has been investigated by using macroscopic continuous models. If the three competing species disperse randomly, the situation can be described by the following competition-diffusion system of Lotka–Volterra type (e.g., [1, 23]):

$$\begin{cases} u_t = d_1 \Delta u + (r_1 - u - b_{12}v - b_{13}w)u \\ v_t = d_2 \Delta v + (r_2 - v - b_{21}u - b_{23}w)v \\ w_t = d_3 \Delta w + (r_3 - w - b_{31}u - b_{32}v)w, \end{cases} \quad (1)$$

where $u(x, t)$, $v(x, t)$ and $w(x, t)$ are respectively the population densities for the three competing species U , V and W for space x and time t . The parameters d_i , r_i and b_{ij} ($i, j = 1, 2, 3, i \neq j$) denote respectively the diffusion rates, the intrinsic growth rates and the inter-specific competition rates. All of them are positive constants. With this model formulation, we note that the maximum density for the i -th species, i.e., the concentration the species would naturally reach in the absence of other competitors (carrying capacity), is given by r_i ($i = 1, 2, 3$). From now on, to simplify the notation we will denote the growth term of the equation for u by

$$f_1(u, v, w) = (r_1 - u - b_{12}v - b_{13}w)u.$$

Similarly, we will denote by f_2 and f_3 the growth terms for the v and w equation, respectively. System (1) is usually considered in a bounded domain Ω with the initial and boundary conditions

$$u(x, 0) = u_0(x), \quad v(x, 0) = v_0(x), \quad w(x, 0) = w_0(x), \quad x \in \Omega, \quad (2)$$

and

$$\frac{\partial u}{\partial \nu}(x, t) = 0, \quad \frac{\partial v}{\partial \nu}(x, t) = 0, \quad \frac{\partial w}{\partial \nu}(x, t) = 0, \quad x \in \partial\Omega, \quad t > 0, \quad (3)$$

respectively, where $u_0(x)$, $v_0(x)$ and $w_0(x)$ are given non-negative functions and ν denotes the unit vector normal to the boundary $\partial\Omega$.

Firstly, we explain the behaviour of the two strongly competing species U and V in absence of the exotic species W . In this case, (1) reduces to the well-studied two species competition-diffusion system for U and V

$$\begin{cases} u_t = d_1 \Delta u + (r_1 - u - b_{12}v)u = d_1 \Delta u + f_1(u, v, 0) \\ v_t = d_2 \Delta v + (r_2 - v - b_{21}u)v = d_2 \Delta v + f_2(u, v, 0). \end{cases} \quad (4)$$

We assume that

$$b_{12} > 1 \quad \text{and} \quad b_{21} > 1, \quad (A1)$$

which means that U and V are strongly competing, i.e., *competitive exclusion* [9] occurs between them in the case they cannot move (see for example [20] for a discussion about the competition ODEs obtained by setting $d_i = 0$, $i = 1, 2, 3$). If the domain Ω is convex, any non-constant equilibrium solution of (4) is unstable under the boundary conditions (3) [15] and any positive solution generically converges to either $(r_1, 0)$ or $(0, r_2)$ [11]. This means that competitive exclusion occurs between two strongly competing species, even if they are allowed to move by diffusion in space.

Unfortunately, the results above do not address the more practical and naïve question: *Which species will be surviving after a long time?* In order to answer it, the information given by the one-dimensional traveling wave solution $(u, v)(z)$ ($z = x - \theta_{uv}t \in \mathbb{R}$) with signed velocity θ_{uv} is particularly important. This solution is given by

$$\begin{cases} d_1 u_{zz} + \theta_{uv} u_z + f_1(u, v, 0) = 0, & z \in \mathbb{R} \\ d_2 v_{zz} + \theta_{uv} v_z + f_2(u, v, 0) = 0, & z \in \mathbb{R} \end{cases} \quad (5)$$

with the boundary conditions

$$\begin{cases} \lim_{z \rightarrow -\infty} (u(z), v(z)) = (r_1, 0) \\ \lim_{z \rightarrow +\infty} (u(z), v(z)) = (0, r_2). \end{cases} \quad (6)$$

It is known that the solution $(u(z), v(z))$ to (5)–(6) with velocity θ_{uv} is unique (up to translations) and stable [14].

From now on we assume

$$\theta_{uv} > 0, \quad (A2)$$

which indicates that U is stronger than V when they move by diffusion, since V asymptotically occupies the whole domain. If we had that $\theta_{uv} < 0$, the situation would be reversed so that U would go extinct. In the case $\theta_{uv} = 0$ instead, the traveling wave does not give any further information on the dynamics of U and V . However, even in this last case, in one-dimensional bounded domains we expect that the interface between U and V moves, since only one species can eventually survive, being there

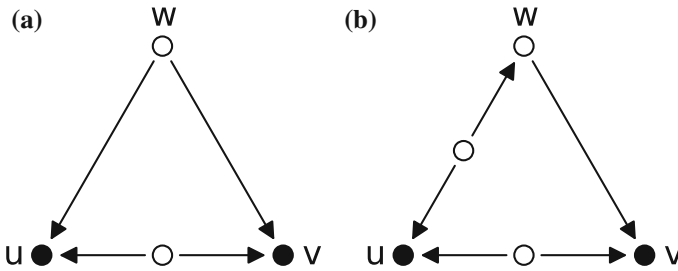


Fig. 1 Equilibria and linear stability for the system of ODEs associated to (1). The points u, v and w denote respectively the equilibria $(r_1, 0, 0), (0, r_2, 0)$ and $(0, 0, r_3)$. *Black and white dots* denote respectively linear stability and instability of equilibria in the three-species system, while *arrows* denote stability in each two-species subsystem. **a** Equilibria for small values of r_3 **b** Equilibria for intermediate values of r_3

no non-constant stable equilibria. In two-dimensional domains (both bounded and unbounded) instead, the motion of the front is driven mostly by curvature effects [8].

We now consider the situation where an exotic species W invades the native (U, V) system. We are interested in investigating whether and in which situations competitor-mediated coexistence occurs in (1)–(3). Along this direction, the coexistence problem has already been discussed in presence of cyclic competition among the three species U, V and W [1, 7]. In this paper we consider a different situation, that is, an exotic species W which is *weaker* than the other two. This setting can be classified into two cases. One possibility is that W is absolutely weaker than both U and V in the sense that

$$\frac{r_1}{r_3}b_{31} > 1 > \frac{r_3}{r_1}b_{13} \quad \text{and} \quad \frac{r_2}{r_3}b_{32} > 1 > \frac{r_3}{r_2}b_{23}, \tag{7}$$

as shown schematically in Fig. 1a. For example, this situation is achieved by choosing r_3 suitably small while keeping all the other parameters fixed. In such case, one can intuitively expect that competitor-mediated coexistence does not occur, although this has not been proved analytically.

The other case is that W is absolutely weaker than V but strongly competing (not absolutely stronger as in [1]) with U in the sense that

$$\frac{r_2}{r_3}b_{32} > 1 > \frac{r_3}{r_2}b_{23}, \quad \frac{r_3}{r_1}b_{13} > 1 \quad \text{and} \quad \frac{r_1}{r_3}b_{31} > 1. \tag{A3}$$

This situation can be achieved for intermediate values of r_3 (the exact range depending on the values of the other parameters). In this case, (A1) and (A3) imply that, in the ODEs associated to (1), $(r_1, 0, 0)$ and $(0, r_2, 0)$ are locally stable, while $(0, 0, r_3)$ is saddle-type unstable, as shown in Fig. 1b. In addition to these conditions, if we require any positive equilibrium of the ODEs to lie outside the domain of values admissible as densities (i.e., non-negative values smaller than the carrying capacities) or to be unstable, then it is known that in general any positive solution $(u(t), v(t), w(t))$ of the ODEs tends to either $(r_1, 0, 0)$ or $(0, r_2, 0)$ [12, 27]. This means that, in the sense of ODEs, W does not influence the dynamics of U and V asymptotically and thus competitor-mediated coexistence cannot occur. This result also holds when spatial

dispersal is added if all diffusion rates are very large [4]. This conclusion seems to be obvious because W is *weaker* in (U, V, W) system.

However, our recent paper [17] emphasizes that, if the diffusion rates are not very large, this is not necessarily correct, i.e., it is possible for U and V to coexist dynamically even if W is “weak” in the sense above. Consider the one-dimensional traveling wave solutions associated to the (v, w) and (w, u) subsystems, defined in a similar way to equations (5)–(6), and denote the velocities of such traveling waves by θ_{vw} and θ_{wu} , respectively. In the case of the monostable subsystem (v, w) one knows that the velocity θ_{vw} of any traveling wave must be positive, since the equilibrium $(0, r_3)$ is unstable [13]. In the case of the bistable subsystem (w, u) the sign of the (unique) velocity θ_{wu} depends on the parameter values. As an additional assumption, we will require that

$$\theta_{wu} > 0. \quad (\text{A4})$$

Assumptions (A1–4) imply that we have cyclic competition as defined in [1], even if the underlying system considered here has a very different structure. This means that when each couple of species is considered in absence of the other one, U results stronger than V , V stronger than W and W stronger than U in space. Thus we may imagine the possibility that the V species, which is weaker in the absence of the invader W , becomes able to overcome U by cooperating with W , and that competitor-mediated coexistence occurs.

In order to show that competitor-mediated coexistence of U and V is indeed possible, we will numerically solve the problem (1)–(3) for the following parameter values:

$$\begin{aligned} d_1 = d_2 = d_3 = 1, \quad r_1 = r_2 = 28, \\ b_{12} = \frac{22}{21}, \quad b_{13} = 4, \quad b_{21} = \frac{37}{21}, \quad b_{23} = \frac{3}{4}, \quad b_{31} = \frac{26}{21}, \quad b_{32} = \frac{22}{21}. \end{aligned} \quad (8)$$

The intrinsic growth rate r_3 of the invading species W is taken to be a free parameter. Its role can be ecologically interpreted as follows: The larger r_3 (respectively smaller), the more favourable (respectively hostile) the environment for the invader W . For this reason, we expect r_3 to play an important role in making competitor-mediated coexistence possible. With the parameters values as in (8), we must take r_3 in the interval $(7, 29 + 1/3)$ in order to enforce (A3). In addition, we note that in the sub-interval $(21 + 147/529, 28 + 140/373)$ an admissible positive constant equilibrium solution exists but is unstable.

We consider (1)–(3) in a rectangular domain Ω . Suppose that the species U (respectively V) is initially placed at full carrying capacity in the left (respectively right) half of Ω . Then, in the absence of W competitive exclusion happens between U and V , so that the interface between them moves towards the right with U displacing V . This means that, in the absence of W , the whole domain will be occupied in the long run by the sole species U . Now consider the situation in which the exotic species W invades a small bounded region around the interface between U and V , as shown in Fig. 2. The resulting behaviour of U , V and W for different values of r_3 is shown in Figs. 3, 4, 5, 6, which demonstrate that either competitive exclusion or competitor-mediated coexistence occurs, sensitively depending on the value of r_3 . When r_3 is relatively

Fig. 2 Initial conditions (2) consisting of an interface between regions dominated respectively by U and V being perturbed by the invasion by the exotic species W . The red (respectively green) colour denotes regions occupied mainly by U (respectively V), while the blue colour denotes regions where W is not negligible (W is nowhere the dominant species)

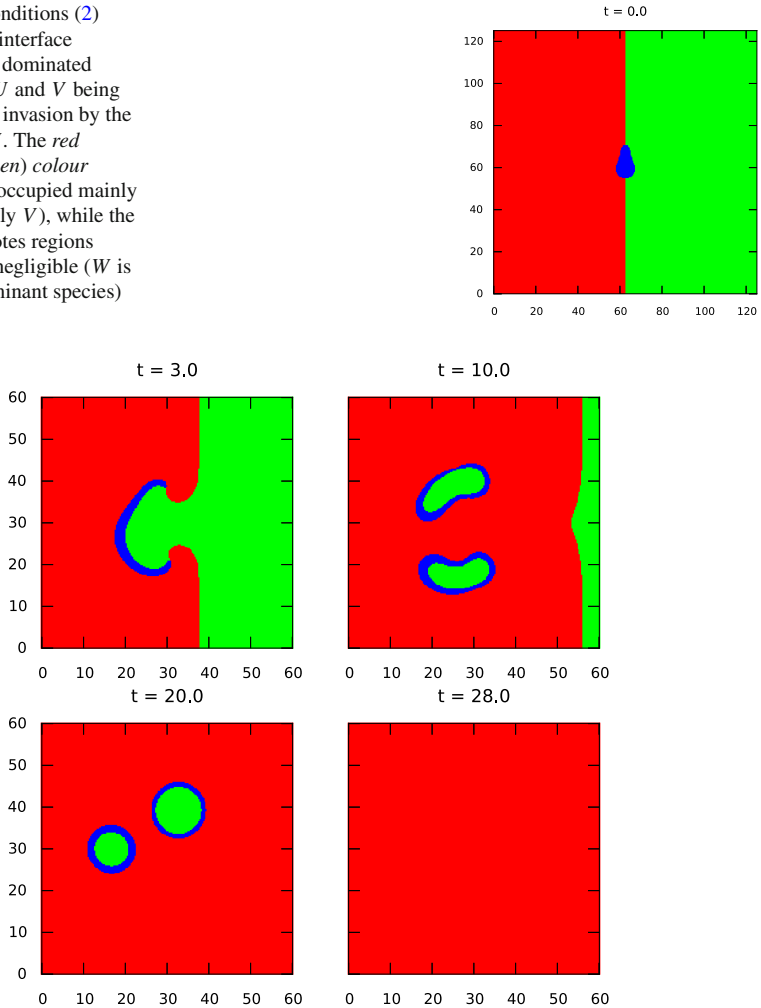


Fig. 3 Competitive exclusion for $r_3 = 27$ and other parameters specified as in (8)

small ($r_3 = 27$), U eventually prevails on the other species, as it is expected since W is too weak to take hold in the new habitat, and competitor-mediated coexistence does not occur, as shown in Fig. 3. For intermediate values of r_3 ($r_3 = 27.12$ and 27.5) the behaviour drastically changes, as shown in Figs. 4 and 5, and the three species coexist dynamically. We remark that, even in this parameter range, certain initial conditions (for example when the area initially occupied by W is too small or far away from the interface between U and V) do not lead to coexistence. When r_3 is relatively large ($r_3 = 28.3$), we have again competitive exclusion, as shown in Fig. 6, but in this case V is the only species that eventually survives. We emphasize that the invasion by W has thus reversed the natural competition relation between U and V : V becomes the dominant species (compatibly with the initial conditions), even

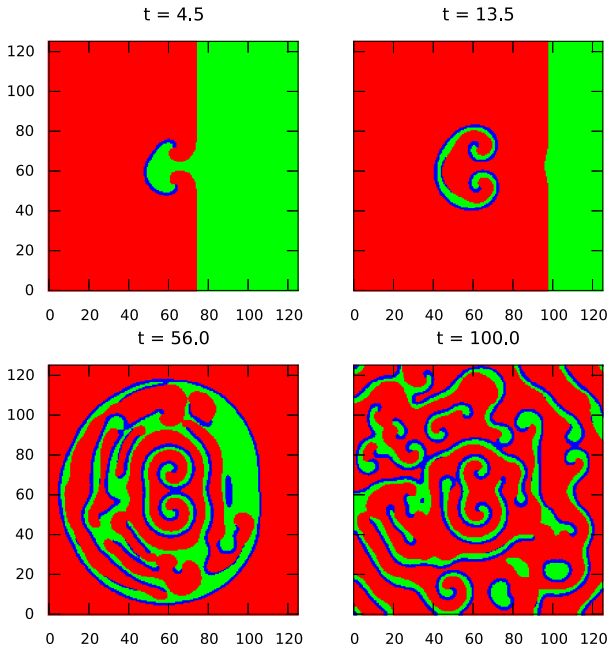


Fig. 4 Dynamic coexistence for $r_3 = 27.12$ and other parameters specified as in (8)

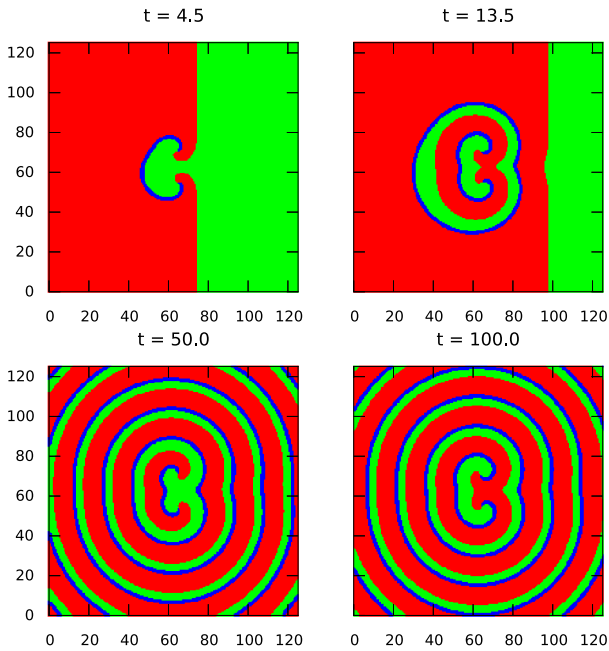
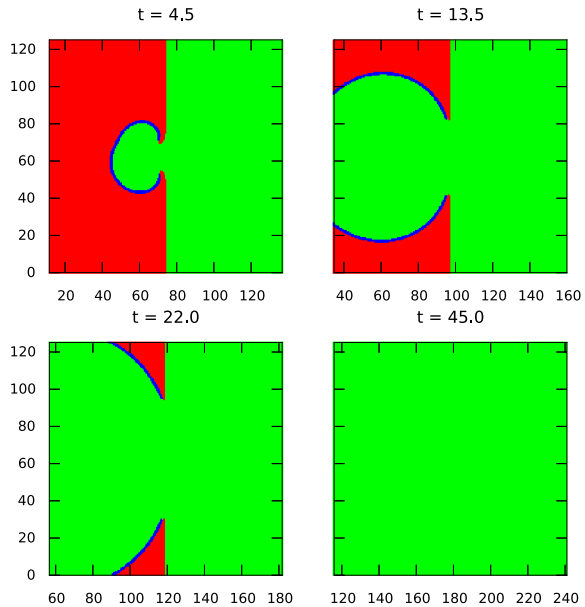


Fig. 5 Dynamic coexistence for $r_3 = 27.5$ and other parameters specified as in (8)

Fig. 6 Competitive exclusion for $r_3 = 28.3$ and other parameters specified as in (8). Here the reference frame is moving with the same velocity of the interface between U and V , in order to track the wedge-shaped features as they move



if in the absence of W it was normally doomed to extinction. Observing Figs. 4, 5 and 6, we notice that such diverse spatio-temporal patterns are produced by the delicate interaction of two different kinds of propagating waves involving the species (U, V) and (U, V, W) , respectively. In particular, Fig. 6 exhibits that the transient behaviour distinctive of the reversal of roles between U and V consists in wedge-shaped patterns originating from the destructive interaction of two fronts of different type.

In this paper, we are concerned with the study of the interaction of these two kinds of propagating fronts composed respectively by the species (U, V) and (U, V, W) . In particular, we are interested in how their behaviour changes as the value of the free parameter r_3 varies. We will firstly consider the one-dimensional case and then show how the extension to two dimensions produces several interesting novel patterns, such as the moving wedges shown in Fig. 6.

2 Interaction of propagating fronts

2.1 One-dimensional traveling wave solutions

We first note that, under assumptions (A1–4), (1) is a bistable system in the sense that $(r_1, 0, 0)$ and $(0, r_2, 0)$ are locally stable. In this section, we study the existence of one-dimensional traveling wave solutions which connect $(r_1, 0, 0)$ and $(0, r_2, 0)$ at infinities. These traveling wave solutions $(u(z), v(z), w(z))$ ($z = x - \theta t$) with signed velocity θ satisfy

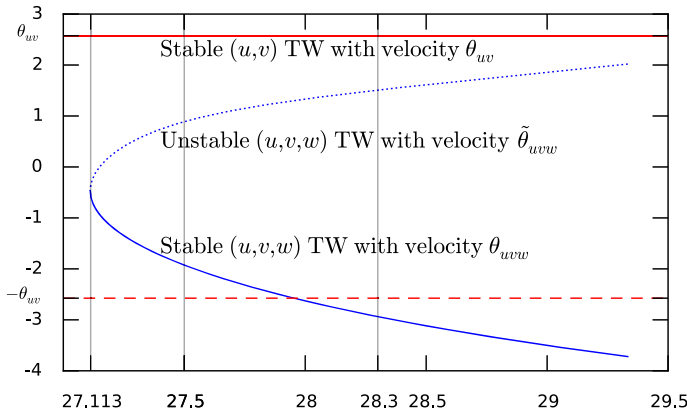


Fig. 7 Global structure of the solutions to (9)–(10) for the parameters given in (8) and with r_3 taken to be a free parameter. The horizontal axes and the vertical axes are respectively the parameter r_3 and the velocity θ of the traveling waves. The branch corresponding to the stable trivial traveling wave is in solid red, while the branch of the non-trivial ones is in blue

$$\begin{cases} d_1 u_{zz} + \theta u_z + f_1(u, v, w) = 0, & z \in \mathbb{R} \\ d_2 v_{zz} + \theta v_z + f_2(u, v, w) = 0, & z \in \mathbb{R} \\ d_3 w_{zz} + \theta w_z + f_3(u, v, w) = 0, & z \in \mathbb{R} \end{cases} \tag{9}$$

with the boundary conditions

$$\begin{cases} \lim_{z \rightarrow -\infty} (u(z), v(z), w(z)) = (r_1, 0, 0) \\ \lim_{z \rightarrow +\infty} (u(z), v(z), w(z)) = (0, r_2, 0). \end{cases} \tag{10}$$

Obviously, the problem (9)–(10) has a non-negative and bounded solution given by $(u(z), v(z), 0)$ and having velocity $\theta = \theta_{uv} > 0$, which is independent of r_3 , where $(u(z), v(z))$ is the unique solution of (5)–(6). We call it the one-dimensional *trivial* traveling wave solution of (1). It is noted that the trivial traveling wave is stable in the full system (Ikeda, personal communication (2006)).

A natural question is whether or not the system (1) admits *non-trivial* traveling wave solutions, i.e., solutions of (9)–(10) in which $w(z)$ is not zero everywhere. We are especially interested in the existence and velocity θ of such solutions as r_3 varies. Using the numerical continuation software AUTO [6], we can solve (9)–(10) and draw the global structure of the traveling wave solutions as r_3 is varied, as shown in Fig. 7. When r_3 is relatively small (say, $r_3 = 27$), Fig. 7 indicates that there is no non-trivial traveling wave solution. On the other hand, as r_3 increases, a saddle-type bifurcation appears, so that two non-trivial traveling waves are generated, one of which is stable with velocity θ_{uvw} and the other is unstable with velocity $\tilde{\theta}_{uvw}$. We find that $\theta_{uvw} < 0$, which means that, thanks to the presence of W , the direction of propagation is reversed in the non-trivial stable traveling wave. This indicates that V drives U to extinction everywhere as $t \rightarrow \infty$. The three traveling wave solutions for $r_3 = 28.3$ are reported in Fig. 8. Unfortunately, the analytical proof of existence and stability of non-trivial

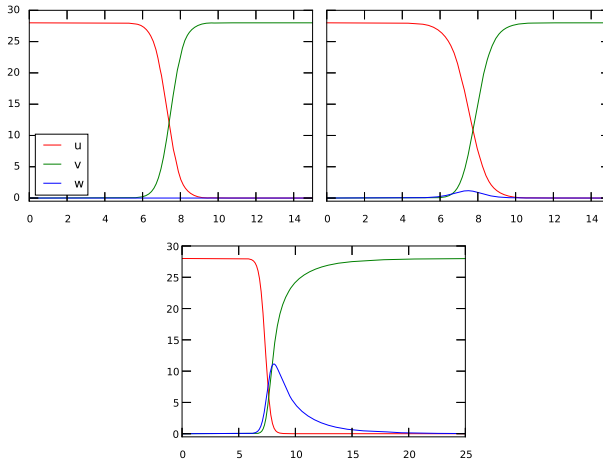


Fig. 8 Profiles of the solutions to (9)–(10) when $r_3 = 28.3$ and the other parameters are specified as in (8). From left to right, the trivial traveling wave ($\theta_{uv} = 2.575$), the unstable non-trivial one ($\theta_{uvw} = 1.509$) and the stable non-trivial one ($\theta_{uvw} = -2.938$) are reported, where u, v and w are drawn in red, green and blue, respectively

solutions to (9)–(10) is still open. In the following, we will denote the speeds of the two stable one-dimensional traveling waves as $c_{uv} = |\theta_{uv}|$ and $c_{uvw} = |\theta_{uvw}|$.

Another important property is the planar stability of these two stable traveling wave solutions with speeds c_{uv} and c_{uvw} . We numerically confirm that both are planarly stable in two dimensions when $d_1 = d_2 = d_3 = 1$, as is the case for (8). However, we note that planar stability does not necessarily hold for different values of the diffusion rates [17]. We assume that all stable one-dimensional traveling wave solutions which are discussed in this paper are also planarly stable.

2.2 Interaction of traveling waves in one spatial dimension

Before considering the interaction of two propagating fronts in two spatial dimensions, whose resulting behaviour has been anticipated in Figs. 4, 5 and 6, we need to firstly study what happens in one dimension. There are several ways in which the two different kinds of stable one-dimensional traveling waves shown in the previous section may interact.

- (i) **Interaction of trivial traveling waves:** The waves in this case move in opposite directions with the same speed c_{uv} . The waves approach each other and are annihilated on collision, so that the final state as $t \rightarrow \infty$ is the equilibrium $(r_1, 0, 0)$ (see Fig. 9) [18].
- (ii) **Interaction of non-trivial traveling waves:** Also in this case the waves move in opposite directions, but the common speed is now c_{uvw} . Similarly to (i), annihilation of the waves occurs, so that the final state as $t \rightarrow \infty$ is $(0, r_2, 0)$ (see Fig. 10).

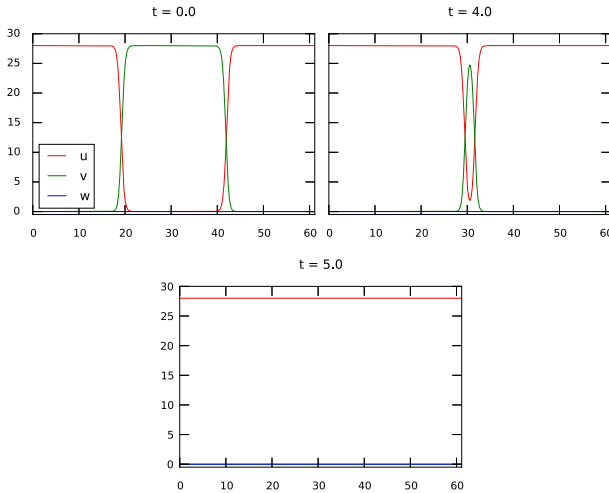


Fig. 9 Annihilation of one-dimensional trivial waves

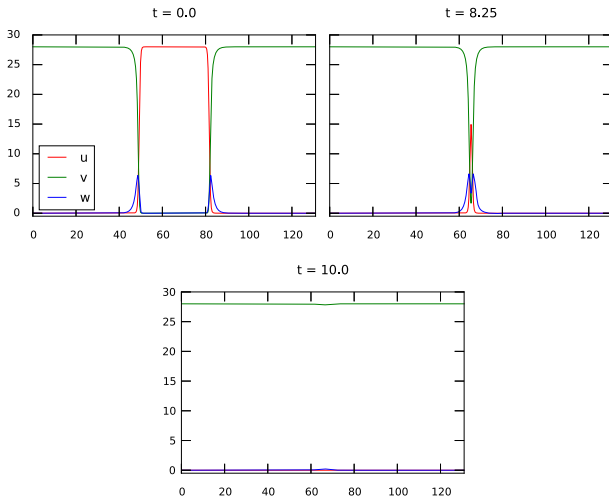


Fig. 10 Annihilation of one-dimensional non-trivial waves for $r_3 = 27.5$

(iii) **Interaction of trivial and non-trivial traveling waves:** Assume that both waves move in the positive direction. Several cases have to be distinguished, depending on the relative position and relative speed of the two waves.

(a) *The trivial traveling wave is the leftmost one*

(a-1) $c_{uv} > c_{uvw}$: Fig. 11 ($r_3 = 27.12$) shows that after collision occurs the rightmost wave continues to propagate unaffected, while the leftmost one is replaced by a new non-trivial wave moving in the opposite direction as if it were reflected.

(a-2) $c_{uv} > c_{uvw}$ and $c_{uv} \approx c_{uvw}$: Fig. 12 ($r_3 = 27.5$) shows that the waves merge and a single homoclinic-type traveling wave appears.

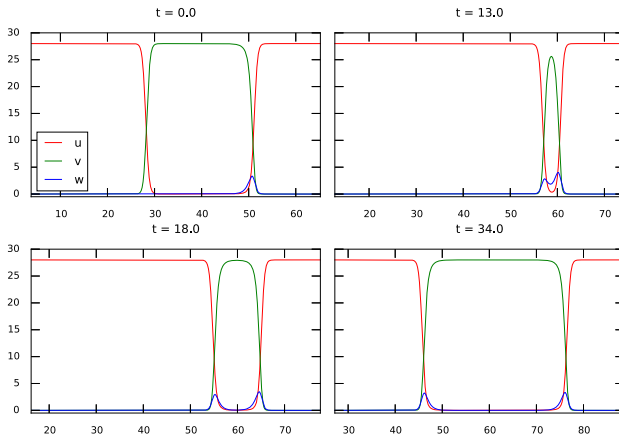


Fig. 11 Reflection of one-dimensional trivial and non-trivial waves for $r_3 = 27.12$

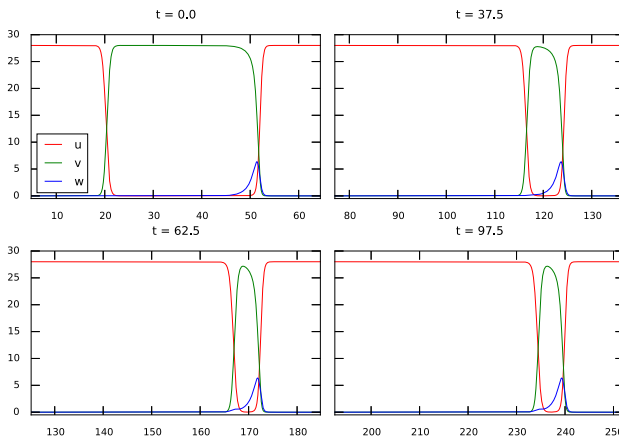


Fig. 12 Occurrence of a homoclinic wave by merging of one-dimensional trivial and non-trivial waves for $r_3 = 27.5$

- (a-3) $c_{uv} < c_{uvw}$: Fig. 13 ($r_3 = 28.3$) shows that the gap between the two waves keeps growing so that nothing happens, in the sense that there is no interaction between the fronts.
- (b) *The non-trivial traveling wave is the leftmost one*
- (b-1) $c_{uvw} < c_{uv}$: As in case (a-3) the waves are non-interacting.
- (b-2) $c_{uvw} > c_{uv}$: Fig. 14 ($r_3 = 28.3$) shows that, differently from cases (a-1,2) above, the two waves are annihilated on collision. In this case too, nothing of interest seems to happen.

Unfortunately, (ii) and (iii) have not been discussed rigorously yet.

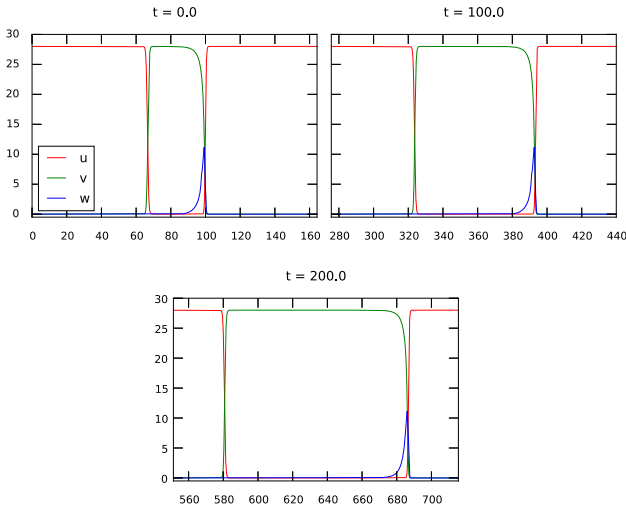


Fig. 13 Non-interacting one-dimensional trivial and non-trivial waves for $r_3 = 28.3$

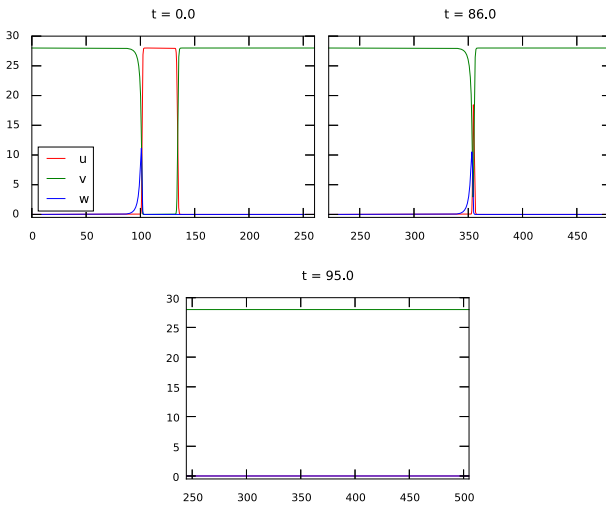


Fig. 14 Annihilation of one-dimensional non-trivial and trivial waves for $r_3 = 28.3$

2.3 Interaction of propagating fronts in two dimensions

When we extend the one-dimensional waves to planar ones, it is obvious to see that the latter interact in the same way as the former. Even in presence of curvature, the basic interactions will (mostly) remain the same. This can give insight in the origin of the patterns produced from the initial conditions shown in Fig. 2.

We start by noting that, in absence of W , the solution will tend to the right-moving planar trivial traveling wave with speed $c_{uv} = 2.575$, independently of the value of r_3 . For $r_3 = 27$, no non-trivial traveling wave exists, as seen in Fig. 7. Thus, when W

invades near the interface between U and V , it is not able to survive for long, since the front profile will tend to the trivial traveling wave, which is the only stable wave in this case. As a result, competitive exclusion occurs and the species U becomes dominant, as shown in Fig. 3.

For $r_3 = 27.12$ instead, a stable non-trivial traveling wave exists and has speed $c_{uvw} = 0.688$, which is quite smaller than c_{uv} . This corresponds to case (a-1) and the situation is drastically changed. The reflection of colliding fronts generates additional spiral cores other than the central ones and the delicate balance between the spiral dynamics and the reflection/annihilation of fronts generates the complex spatio-temporal patterns shown in Fig. 4. We observe that in this case reflection is not perfectly attained, i.e., the reflected front reverses direction a second time, transforming back into a trivial front. This is due to the fact that, since in presence of curvature the fronts are not parallel when they interact, the actual relative speed of the fronts is reduced enough for reflection not to successfully occur. We will discuss this phenomenon again later in Sect. 4.

For $r_3 = 27.5$, $c_{uvw} = 1.925$ is just slightly smaller than c_{uv} . This corresponds to case (a-2). In this case we know that colliding fronts merge in a homoclinic one, giving rise to a wave train in one dimension. Then, a pair of spiral waves appears in two dimensions, as shown in Fig. 5. This behaviour is the same exhibited by the Belousov Zhabotinsky chemical reaction [19].

Finally, for $r_3 = 28.3$ we have that $c_{uvw} = 2.938$ is larger than c_{uv} , which corresponds to case (a-3), so that the two fronts annihilate on collision in one dimension. However, unlike the previous cases in which the knowledge of one-dimensional behaviour gave us important clues about the patterns appearing in two dimensions, in this case giving a prediction is more difficult, since in one dimension no structure is left after annihilation. Instead, the fact that the interaction happens in two spatial dimensions now plays a fundamental role. As we already observed, unless the fronts are planar and parallel, they collide at a certain angle. As a result, annihilation does not happen instantly on the whole length of the interface, but the points where destructive interaction occurs move roughly in a straight line, giving rise to two moving wedge-like patterns, as shown in Fig. 6. This last case suggests us the following conjecture: *A two-dimensional wedge-shaped traveling wave solution of (1) exists if the condition $c_{uv} < c_{uvw}$ is satisfied.*

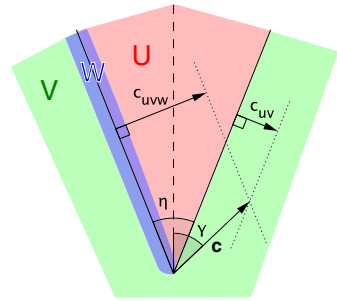
In the next sections, we will investigate numerically whether this conjecture holds or not and discuss the mechanism behind the appearance of such waves.

3 Wedge-shaped traveling waves in two dimensions

3.1 Appearance of a wedge-shaped traveling wave

In the previous section, we have shown that the interaction of the stable non-trivial and trivial waves of (1) produces diverse patterns in two spatial dimensions. We have also emphasized that the pattern properties are mainly due to the type of wave interaction, which depends on the ratio between the velocities of the one-dimensional traveling waves, which is in turn a function of the free parameter r_3 . In this section, assuming

Fig. 15 Structure of an asymmetric wedge-shaped traveling wave with velocity \mathbf{c} . η is the angle between the planar fronts constituting the sides of the wedge, while γ is the angle between the wedge bisector and the direction of the velocity \mathbf{c}



that $c_{uv} < c_{uvw}$, which is the case for relatively large values of r_3 (see Fig. 7), we focus on wedge-shaped traveling wave solutions which propagate in \mathbb{R}^2 with constant velocity and constant shape.

In one dimension, there is no interaction when a trivial traveling wave approaches a non-trivial wave from behind, since the gap between the two steadily increases. Conversely, when the faster non-trivial wave is the back wave and the slower trivial wave is the front one, they approach each other and are annihilated on collision, as shown in Fig. 14. We remark that in both interactions nothing interesting happens in one dimension. However, if (1) with $r_3 = 28.3$ and the other parameters as in (8) is considered in two dimensions, we observe characteristic wedge-like patterns, as shown in Fig. 6. This suggests the existence of truly two-dimensional traveling wave solutions of the equation (1) in \mathbb{R}^2 . These waves would arise from the destructive interaction of two planar fronts and, as a result, have a wedge-like shape, as shown schematically in Fig. 15. The back side of such wedge would consist of the faster non-trivial wave moving towards the inside of the wedge, while its front side would be made up by the trivial wave directed outwards. In the neighborhood of the wedge tip, the planar fronts collide and annihilate each other, as is expected from one-dimensional interaction behaviour. Rather surprisingly, the wedge in its entirety appears to move at a constant velocity without changing shape.

Existence results for truly two-dimensional traveling wave solutions are still scarce. For example, the Allen–Cahn equation has been shown to possess simple wedge-shaped traveling wave solutions [22]. This equation admits only one kind of *stable* traveling wave, which interacts destructively with itself. Thus a wedge can be built, but its sides are both made up by the *same* stable wave. As a result, the traveling wave is *symmetric* with respect to the wedge bisector and its velocity also lies on such bisector. Recently, this result has been extended to the two-species competition-diffusion system [21], showing the existence of symmetric-wedges composed by the sole trivial front, which, as we have seen in Fig. 9, interacts destructively with itself. For these two kinds of wedges, the angle between the fronts can assume any value between 0 and π , i.e., we can have a symmetric wedge as long as its front velocities are directed inwards.

The essential difference between our system (1) and the two systems mentioned above is that in our case two distinct stable traveling waves are present instead of only one. Thus, the velocity of our wedge-shaped wave has not to obey the same restrictions,

that is, its direction is different from the wedge bisector and forms with it an angle γ , as shown in Fig. 15. To our knowledge, the occurrence of such *non-symmetric* wedge-shaped traveling waves in reaction-diffusion systems has never been observed before.

If such wedge-shaped traveling waves exist in \mathbb{R}^2 , given the speeds c_{uv} and c_{uvw} associated to its sides, the following questions arise naturally:

(Q1) What is the angle between the two sides of the wedge?

(Q2) What is the velocity of the traveling wave?

(Q3) In particular, what is the direction of such velocity?

(Q2-3) will be answered in the next section. For the answer to (Q1), we will rely on numerical simulation to gather evidence on the existence of such asymmetric wedge-shaped traveling waves as the angle between the planar fronts varies.

3.2 The velocity of wedge-shaped traveling waves

In [26] a relation among the wedge angle η , the speeds c_{uv} and c_{uvw} of the constituent planar waves and the velocity \mathbf{c} of the wedge-shaped traveling wave has been proposed. Such relation has been obtained by assuming that each planar front propagates independently at its own speed and computing the velocity of the wedge tip, i.e., of the intersection point of the two fronts. Geometrically, this procedure can be carried out by tracing a parallel line to each front at a distance equal to the front speed, as shown in Fig. 15. Then, if this conjecture is correct, the vector connecting the wedge tip to the intersection of these two lines is the velocity of the wedge-shaped traveling wave.

We remark that no information relative to the competition term of the equation is used (except what is already contained in the front speeds), so that the same formula can be extended to other systems, if they admit a couple of stable planar fronts which interact destructively. Suppose that a reaction-diffusion system admits a wedge-shaped traveling wave solution with velocity \mathbf{c} such that the angle between the sides is η and the speed of the planar front associated to the left (respectively right) side is θ_l (respectively θ_r). We consider θ_l and θ_r to be signed speeds: a positive value indicates that the corresponding front velocity is directed towards the inside of the wedge. In the simple case of the symmetric wedge-shaped waves shown in [21], both sides are composed by inward-moving trivial planar fronts, so that we have $\theta_l = \theta_r = c_{uv} > 0$. In the case of the hypothetical asymmetric wedge-shaped traveling wave shown in Fig. 15, we have that the left side of the wedge is made up by a non-trivial planar wave moving inwards, i.e., $\theta_l = c_{uvw} > 0$, while the right side consists of a trivial planar wave moving outwards, i.e., $\theta_r = -c_{uv} < 0$.

The speed and direction formulas for wedge-shaped traveling waves are then explicitly given by

$$|\mathbf{c}|^2 = \frac{\theta_l^2 + \theta_r^2 + 2\theta_l\theta_r \cos \eta}{\sin^2 \eta}, \quad (11)$$

$$\tan \gamma = \frac{\rho - 1}{\rho + 1} \tan \frac{\eta}{2}, \quad (12)$$

where γ is the angle between the wedge bisector and the direction of \mathbf{c} (γ increases clockwise), as shown in Fig. 15, and ρ is the signed speed ratio θ_l/θ_r . Note that in the case of an asymmetric wedge-shaped traveling wave we have that $\rho < 0$.

Another possible justification to (11)–(12) can be given directly from the traveling wave equation. Consider a generic reaction-diffusion system

$$\mathbf{u}_t = \mathbf{D}\Delta\mathbf{u} + \mathbf{f}(\mathbf{u}) \quad \text{in } [0, T] \times \mathbb{R}^2, \quad (13)$$

where $\mathbf{u} : [0, T] \times \mathbb{R}^2 \rightarrow \mathbb{R}^m$ (m is the number of equations), $\mathbf{D} \in \mathbb{R}^{m \times m}$ is a positive diagonal matrix containing the diffusion coefficients and $\mathbf{f} : \mathbb{R}^m \rightarrow \mathbb{R}^m$ is the reaction term. Being a traveling wave solution of (13) with velocity \mathbf{c} means solving

$$\mathbf{D}\Delta\mathbf{U} + \nabla\mathbf{U}\mathbf{c} + \mathbf{f}(\mathbf{U}) = \mathbf{0} \quad \text{in } \mathbb{R}^2, \quad (14)$$

where $\nabla\mathbf{U} : \mathbb{R}^2 \rightarrow \mathbb{R}^{m \times 2}$ is the Jacobian of \mathbf{U} .

First, we remark that the velocity of a planar traveling wave is not unique, in the sense that, given a planar wave with shape \mathbf{U}_p associated to a one-dimensional wave with speed c_{TW} , $(\mathbf{U}_p, \mathbf{c}_p)$ solves the traveling wave equation (14) for any vector \mathbf{c}_p whose normal component with respect to the front is equal to c_{TW} . From now on, among the admissible velocities of a planar traveling wave we take the velocity \mathbf{c}_p oriented along the normal to the front, whose modulus is equal to the one-dimensional wave speed c_{TW} .

Let $\mathbf{U} : \mathbb{R}^2 \rightarrow \mathbb{R}^m$ be a traveling wave solution of (13) with speed \mathbf{c} . Suppose that there exists a planar traveling wave $(\mathbf{U}_l, \mathbf{c}_l)$ of (13) such that in some asymptotic direction the shape of \mathbf{U} coincides with the shape of \mathbf{U}_l , as is the case for a side of a wedge-shaped traveling wave. For the sake of simplicity, suppose that it is actually possible to find $\Omega \subset \mathbb{R}^2$ on which \mathbf{U} coincides with \mathbf{U}_l . Then, also $(\mathbf{U}_l, \mathbf{c})$ is a solution of (14) on Ω , which means \mathbf{c} must be one of the possible velocities of the planar wave \mathbf{U}_l . Thus, as discussed in the previous paragraph, we must have $\mathbf{c} - \mathbf{c}_l \perp \mathbf{c}_l$ or equivalently $\mathbf{c}^t \mathbf{c}_l = c_l^2$, where t is the transpose operator. If we have another planar traveling wave $(\mathbf{U}_r, \mathbf{c}_r)$ of (13) satisfying the same conditions, such as the one associated to the other side of the wedge, we obtain a second relation $\mathbf{c}^t \mathbf{c}_r = c_r^2$. By combining both of them, we obtain a linear system whose solution gives us the formulas (11)–(12). In Appendix A we report some propositions formalizing this alternative but equivalent derivation of the velocity of such two-dimensional traveling waves.

The method presented in this section allows us to determine the velocity of a two-dimensional wedge-shaped traveling wave, *assuming* that a wave with such asymptotic behaviour exists. The conditions for the existence of such waves will be investigated in the next section.

3.3 Existence of a critical angle for asymmetric wedge-shaped traveling waves

In order to increase our confidence in the existence of such wedge-shaped traveling waves, we numerically solve the reaction-diffusion system (1) and the associated traveling wave equation in two dimensions. In order to increase the reliability of such

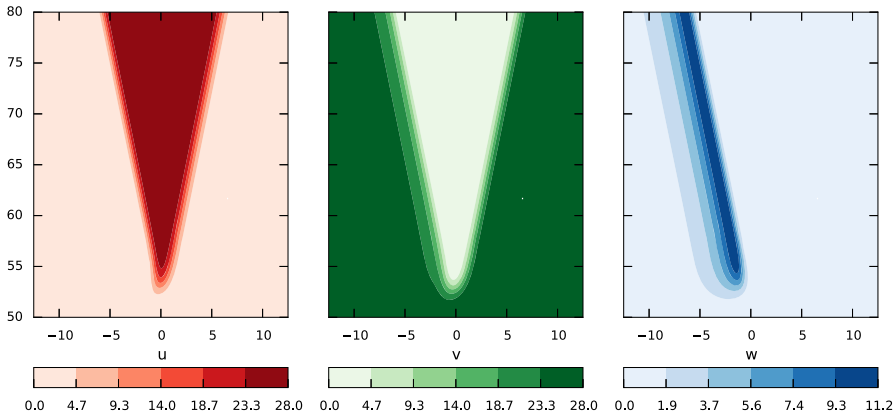


Fig. 16 Asymmetric wedge-shaped traveling wave with angle $\eta = 0.4$, for $r_3 = 28.3$ and the other parameters specified as in (8), obtained by numerically solving the two-dimensional traveling wave equation associated to (1)

results, we employ a better numerical method than the one used in Sect. 1. More details are presented in Appendix B.

Consider “wedge-like” initial conditions obtained by taking the two independent planar fronts corresponding to each wedge side, orienting them so that they form an angle equal to η and placing each of them in one half-plane. We will check if the solution to the time-evolution problem (1)–(2), starting from such initial state, converges to an asymmetric wedge-shaped traveling wave with fixed angle η and constant velocity \mathbf{c} , which we expect to be given by (11)–(12). If we observe such convergence, the resulting traveling wave candidate can be further numerically improved by using it as a starting guess for the two-dimensional traveling wave equation (14).

When η is relatively small (say, $\eta = 0.4$), the procedure explained above yields with good confidence an asymmetric wedge-shaped traveling wave with angle η , as shown in Fig. 16. We only show its shape in the proximity of the tip, since far from it the behaviour tends rapidly to that of independently propagating planar fronts. The computed value for the velocity \mathbf{c} is $(2.81711, 0.92533)$, which compares well against the value $(2.81226, 0.91318)$ derived from one-dimensional front speeds by using (11)–(12). This gives us some numerical support to our conjecture about the existence of asymmetric wedge-shaped traveling waves.

On the other hand, if η is relatively large (say, $\eta = 0.8$) we can no longer observe convergence to a wedge-shaped traveling wave with angle η in the time-evolution problem (1)–(2), as shown in Fig. 17. By repeating the same procedure for different initial values of η , we observe that there seems to exist a threshold value for η over which there is no longer convergence to a traveling wave. We thus expect that the range of values of η for which a corresponding asymmetric wedge-shaped traveling wave exists is limited to values under such threshold. We call such limiting value the *critical angle* and denote it by η_c . As can be seen in Fig. 17, when η is greater than η_c , the wedge angle gradually *decreases* starting from the tip. Surprisingly, the angle near the tip eventually stabilizes and the final tip shape and velocity seem to be independent

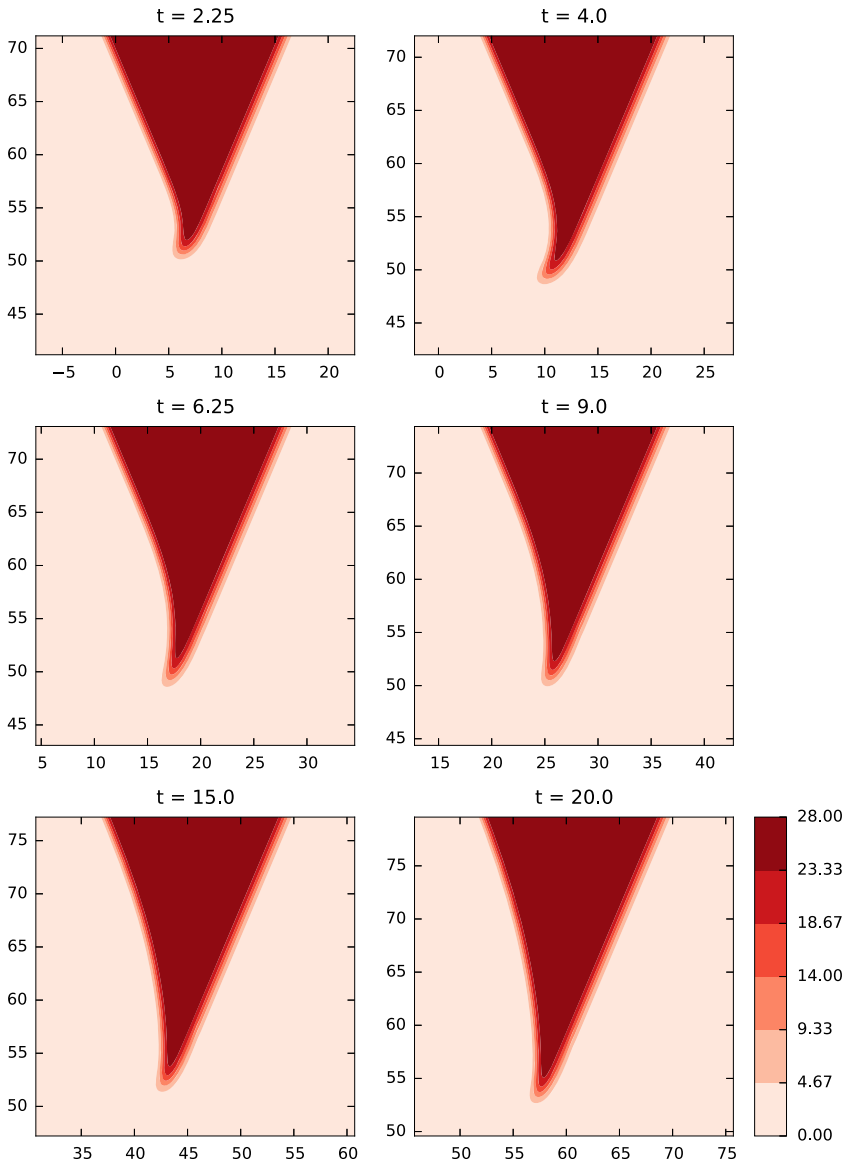


Fig. 17 Evolution in time of a wedge-like pattern with initial angle $\eta = 0.8$, for $r_3 = 28.3$ and the other parameters specified as in (8). The angle gradually decreases, starting from the tip, tending to η_c . Since the reference frame is moving with the expected velocity for a wedge having angle η , the tip, which moves instead with the velocity of the wedge-shaped traveling wave with angle η_c , is gradually left behind

of the initial value of η : According to what one could intuitively expect, this shape and velocity are those of the tip of a wedge-shaped traveling wave with critical angle. We think that, given enough time for the wedge of Fig. 17 to evolve, the sides of the wedge near the tip will straighten up and form an angle equal to η_c . Our conjecture is

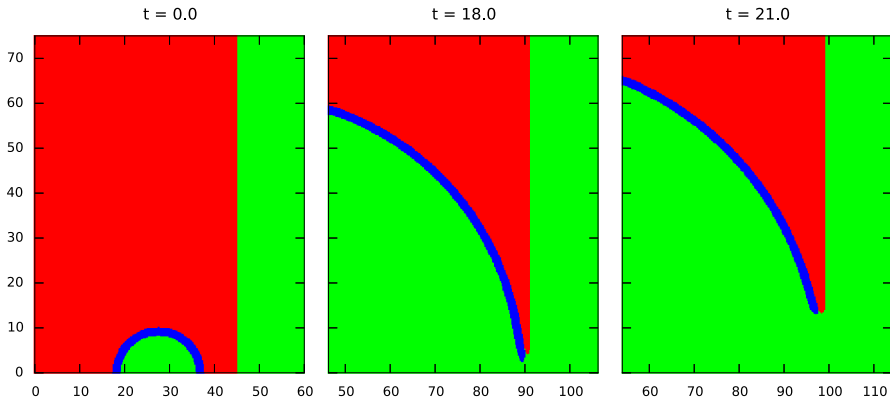


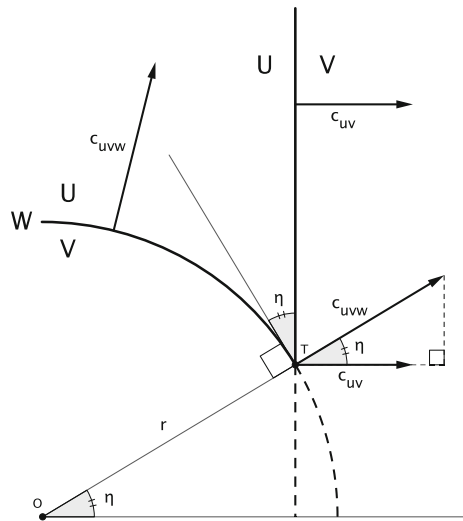
Fig. 18 Interaction of a faster radially expanding non-trivial front with a slower planar trivial front where the parameters are the same as the ones for Fig. 17

thus that, when the initial angle between the wedge sides is larger than η_c , the limit shape of the time-evolution problem (1)–(2) is the wedge-shaped traveling wave with critical angle.

The critical angle η_c arises naturally also in other situations related to wedge-shaped traveling waves. Consider a planar trivial front which is followed by a radially spreading non-trivial front. Their collision results in the creation of a couple of moving wedges. The angle between the wedge sides rapidly *increases* and appears to converge to the critical angle η_c , as shown in Fig. 18, while the tip velocity becomes that of a wedge-shaped traveling wave with critical angle. We remark that this limit behaviour is independent of the front curvature at the time of first interaction, although speed of convergence seems to be dependent on it.

Numerical simulations show that the same critical angle η_c is naturally selected as the angle of wedge-shaped traveling waves in several situations. There may thus be a common principle underlying these phenomena, which may yield a way to compute the critical angle value without resorting to numerical simulations. The simple approximation which sees the fronts as independently propagating and considers their intersection as the wedge tip, while able to give us the correct traveling wave velocity when the wave actually exists, fails to explain why a wedge cannot form with an angle larger than a certain threshold. However, it works unchanged in the situation in which the back front is radially expanding. We start by observing that in this case the angle η of the wedge at its tip is the angle between the planar front and the tangent to the radial front, as shown in Fig. 19. It is also equal to the angle formed by the horizontal direction and the segment connecting the wedge tip with the center of the radial wave. The propagation of the radial front is in general slowed down by curvature effects, but, since the curvature radius increases with time, the speed of such front tends asymptotically to the planar speed c_{uvw} . We will assume that the radius r of the front at time t can be written as $c_{uvw}t - \delta(t)$, with $\delta(t) \rightarrow 0$ as $t \rightarrow \infty$. The horizontal component of the distance between the wedge tip and the center of the radial wave is equal to the position of the planar front, i.e., $c_{uv}t + d$, where d is the distance between the center of the radial wave and the planar front at time $t = 0$. Thus we have that

Fig. 19 Approximation of a radial front catching up with a planar wave, by using independently propagating fronts. O is the center of the radial front; T is the intersection of the two fronts where annihilation occurs, i.e. the tip of the nascent wedge; r is the distance the radial front has propagated; η is the wedge angle at its tip; c_{uv} is the speed of the planar wave; c_{uww} is the speed of the radial front



$\eta(t) = \arccos \frac{c_{uv}t+d}{c_{uww}t-\delta(t)}$, which tends as $t \rightarrow \infty$ to the value $\arccos \frac{c_{uv}}{c_{uww}}$. In conclusion, the approximation by independently moving fronts predicts the appearance of a limit angle whose value is $\eta_c := \arccos \frac{c_{uv}}{c_{uww}}$.

In order to apply this reasoning to the evolution of a wedge-shaped solution with initial angle larger than η_c , a more intuitive explanation of the above derivation can be useful. Note that the horizontal component of the velocity of the radial front is $c_{uww} \cos \eta$. When η is small, this value is larger than c_{uv} and the radial front overtakes the planar one, causing η to increase since the back front is curved. When η reaches η_c , the two velocities are perfectly balanced along the horizontal direction: The angle of the wedge stabilizes and the velocity of the tip no longer changes. Even if curvature effects are accounted for, they result in a smaller propagation speed for the front when the curvature radius is small, which means that balance is achieved at a lower angle. As the curvature radius increases, this angle also increases tending to the critical one.

We may now apply a similar argument to the case of wedge-like initial conditions. We will consider the two sides of the wedge as two independently moving *half-lines*, which are annihilated on collision. For the sake of simplicity, we will orient the right side of the wedge vertically, so that it moves horizontally with speed c_{uv} . Similarly to the previous situation, the velocity of left side has horizontal component equal to $c_{uww} \cos \eta$. When $c_{uww} \cos \eta > c_{uv}$, i.e., $\eta < \eta_c$, the tips of the two half-lines collide and are annihilated, resulting in the normal propagation of the wedge-shaped traveling wave, as shown in Fig. 20a. The same also happens when $\eta = \eta_c$, as shown in Fig. 20b. When $\eta > \eta_c$ instead, the tips do not collide, resulting in no destructive interaction and thus no wedge-shaped traveling wave occurs, as shown in Fig. 20c.

This approximation is not able to describe how initial conditions with angle η larger than η_c evolve to become a wedge with critical angle. Indeed, the boundary between the regions dominated respectively by U and V cannot break in the way shown in Fig. 20c. We have thus to refine our analysis. We start by assuming that each wedge

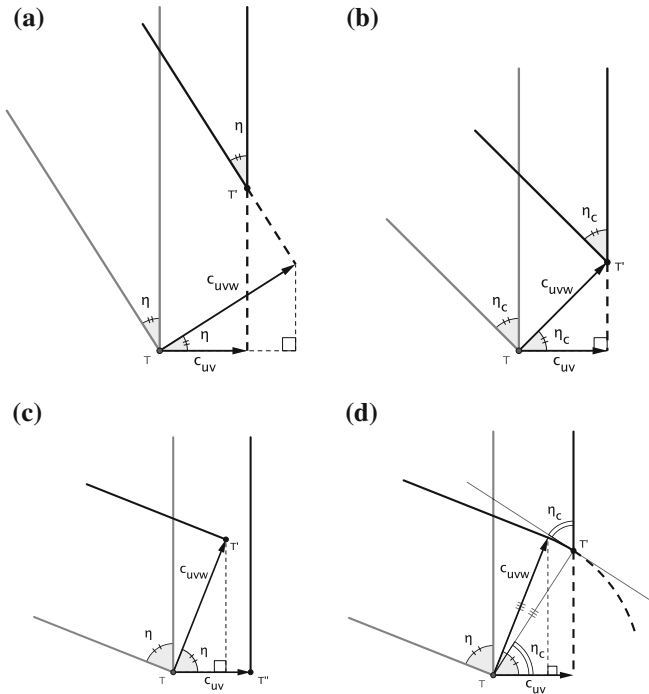


Fig. 20 Approximation of the wedge formation phenomenon by two independently propagating fronts. The point T is the wedge tip at the initial time, while T' (and T'' where present) is the tip after the fronts have moved. The sections of the fronts which have collided and have been annihilated are drawn with *dashed lines*. **a** When $\eta < \eta_c$, the result of independent propagation is still a wedge. **b** When $\eta = \eta_c$, the result of independent propagation is a wedge with velocity $\mathbf{c} = \mathbf{c}_{uvw}$. **c** When $\eta > \eta_c$, the wedge tip splits and the front becomes interrupted, leading to no traveling wedge. **d** When $\eta > \eta_c$, if we assume that the wedge tip becomes the origin of a radial front, in the limit we obtain a wedge with angle equal to η_c .

tip acts as a source of a radial wave, as shown in Fig. 20d. If we neglect curvature effects and assume that the speed of this radial wave is the same as the planar front speed, we obtain that at any subsequent time instant the angle of the wedge tip will be equal to η_c . As time progresses, the curvature of the non-planar part of the back side will decrease, and the shape will tend to a wedge-shaped traveling wave with angle η_c .

However, the simulation in Fig. 17 displays a more complicated transient behaviour. We think that this is due to curvature effects, which slow the propagation of the curved front, originating the curved tip which appears at $t = 4$. As the curvature radius increases, the slowing effect is reduced and the fronts get faster. Eventually they collide, making the curved tip disappear and bringing us back to the case where curvature effects are negligible.

Finally, we remark that our proposed (informal) derivation for the value of η_c is purely geometric in nature and the requirement that the fronts interact destructively does not seem to be essential. A similar constraint on the angle should also appear for colliding planar fronts which interact in different ways, as we will see in the next

section. For the same reasons we expect the appearance of a critical angle in the interaction between planar fronts also in systems other than (1).

4 Other two-dimensional traveling waves arising from planar front interaction

When two parallel planar fronts collide in two dimensions, the resulting interaction is essentially one-dimensional and thus introduces no new phenomena. Novel patterns appear instead from the interaction between a faster radially expanding front and a slower planar front. This is due to the fact that the interaction between the fronts does not occur instantaneously among the whole front length as in the former case. In particular, as we discussed in the previous section, we expect that the angle at which the fronts collide tends to the critical angle and the velocity of the point of interaction becomes constant. These facts hint at the possibility that the patterns produced by such interactions may tend to some two-dimensional traveling wave. Moreover, we would expect similar waves to also exist for any angle of interaction smaller than the critical one.

In the previous section, we have observed this to be true when $c_{uvw} > c_{uv}$: The two different fronts interact destructively in one dimension (Fig. 14), so that the interaction between radial and planar fronts generates a couple of wedge-shaped waves. Now we are interested in investigating what happens when $c_{uv} > c_{uvw}$ and the one-dimensional fronts interact in a different way. We already know that, when $c_{uv} > c_{uvw}$, the possible one-dimensional behaviours are either merging (Fig. 12) or reflection (Fig. 11). In two dimensions we expect that the two colliding fronts become either a single homoclinic front, generating a *zipper-shaped* traveling wave as shown in Fig. 21a, or a couple of fronts moving in opposite directions, generating a *biwedge-shaped* traveling wave as shown in Fig. 21b. Observe that, if such traveling waves exist, their velocities can be

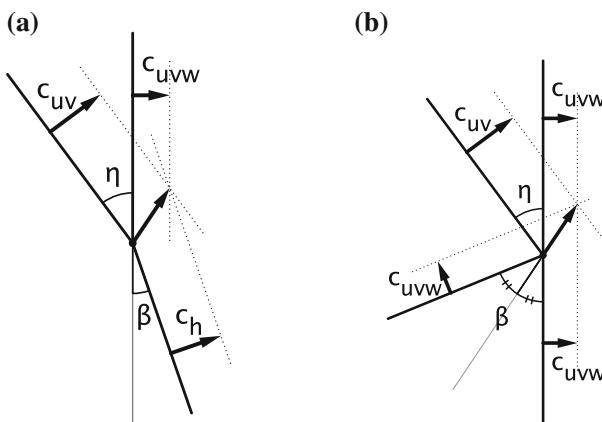


Fig. 21 Schematic structures of two-dimensional traveling waves originating from the interaction of colliding non-parallel planar fronts when $c_{uv} > c_{uvw}$. **a** Zipper-shaped traveling wave solution when interaction in one dimension results in a homoclinic wave with speed c_h . **b** Biwedge-shaped traveling wave solution when interaction in one dimension results in reflection of the fronts

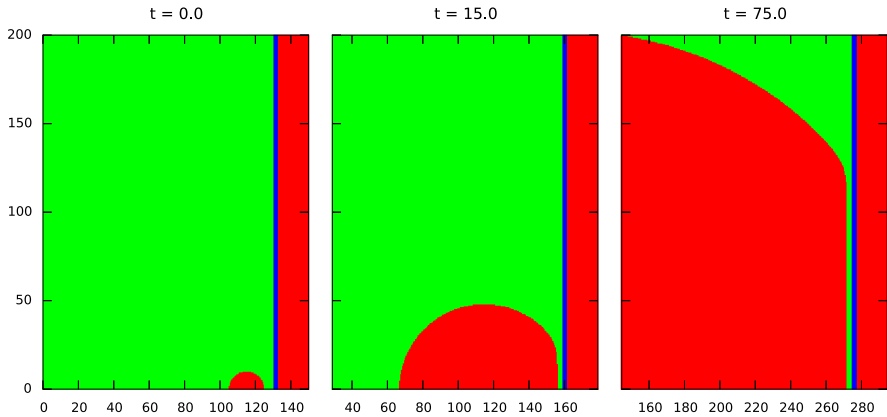


Fig. 22 Interaction of a faster radially expanding trivial front with a slower planar non-trivial front for $r_3 = 27.5$ and the other parameters specified as in (8)

uniquely determined from just the speeds and collision angle of the first two fronts by using (11)–(12). As seen in Sect. 3.2, for any planar front which makes up part of a two-dimensional traveling wave, the relation $\mathbf{c} - \mathbf{c}_p \perp \mathbf{c}_p$ must hold, where \mathbf{c}_p is the normal velocity of such planar front. Thus, as shown in Fig. 21, we can compute easily the directions of propagation for the fronts created after collision. In particular, notice how the bottommost “wedge” in Fig. 21b, which is composed by two non-trivial fronts, is necessarily symmetric with respect to the direction of propagation.

We will now examine the results of radial-planar interaction for several parameter values. In the case $r_3 = 27.5$, there exists a stable homoclinic one-dimensional traveling wave originating from the interaction of the trivial and non-trivial waves and its speed is almost the same as that of the non-trivial front (see Fig. 12). Thus we expect the homoclinic front resulting from two-dimensional interaction to be practically parallel to the non-trivial one, i.e., $\beta = 0$ in Fig. 21a. The numerical simulation of the radial-planar interaction confirms our predictions, as shown in Fig. 22: The angle η between the colliding fronts tends to the critical one and two zipper-shaped waves are generated at the points of collisions. As an example of a zipper-shaped traveling wave for η smaller than the critical angle (in this case $\eta_c \approx 0.726$), a numerical solution of the traveling wave equation is shown in Fig. 23 for $\eta = 0.5$. In the reference frame where the top wedge bisector is oriented vertically, the computed velocity is $(2.33516, 1.28213)$, which is near the value $(2.32216, 1.31286)$ predicted by (11)–(12).

In the case $r_3 = 27.12$, based on the one-dimensional interaction we would expect reflection of the fronts to occur. However, as already noticed in Fig. 4, reflection does not always occur smoothly for two-dimensional curved fronts. Instead, the numerical simulation of the radial-planar interaction reported in Fig. 24 shows that several incomplete reflections happen in succession. The amplitude of these events becomes the smaller the further from the collision point, and as a result the couple of interacting fronts seem to tend to a single homoclinic one. Numerical continuation by AUTO shows that a homoclinic one-dimensional traveling wave exists for $r_3 = 27.12$ and that its speed and the angle observed in Fig. 24 are compatible with the predictions of

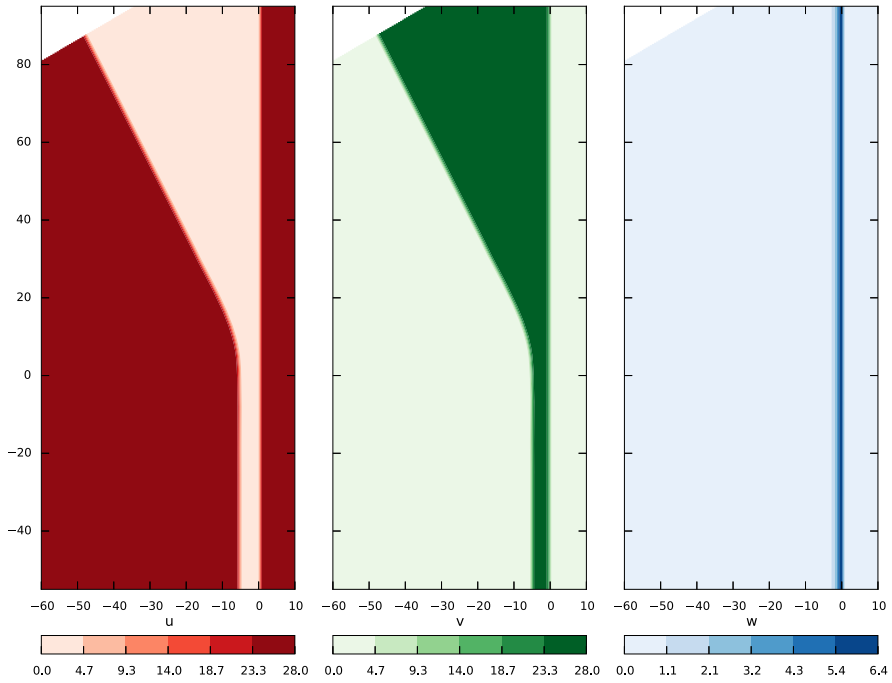


Fig. 23 A zipper-shaped traveling wave arising from the interaction of planar fronts forming an angle $\eta = 0.5$, for $r_3 = 27.5$ and the other parameters specified as in (8), obtained by numerically solving the two-dimensional traveling wave equation associated to (1)

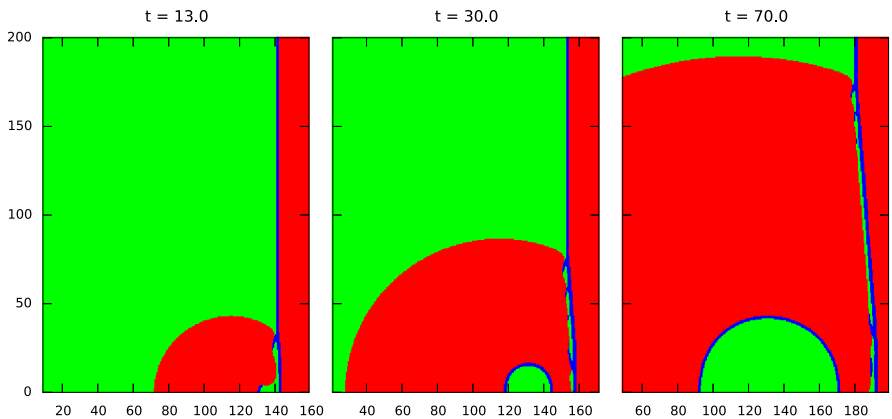


Fig. 24 Interaction of a faster radially expanding trivial front with a slower planar non-trivial front for $r_3 = 27.12$ and the other parameters specified as in (8). Initial conditions are the same as in Fig. 22

Fig. 21a. It seems that also in this case we may have a zipper-shaped traveling wave, although with $\beta \neq 0$ in Fig. 21a. Since the homoclinic wave appears to be *unstable* in one dimension (it splits in two non-trivial waves moving in opposite directions), this hypothetical two-dimensional wave could be unstable as well. A numerical solution

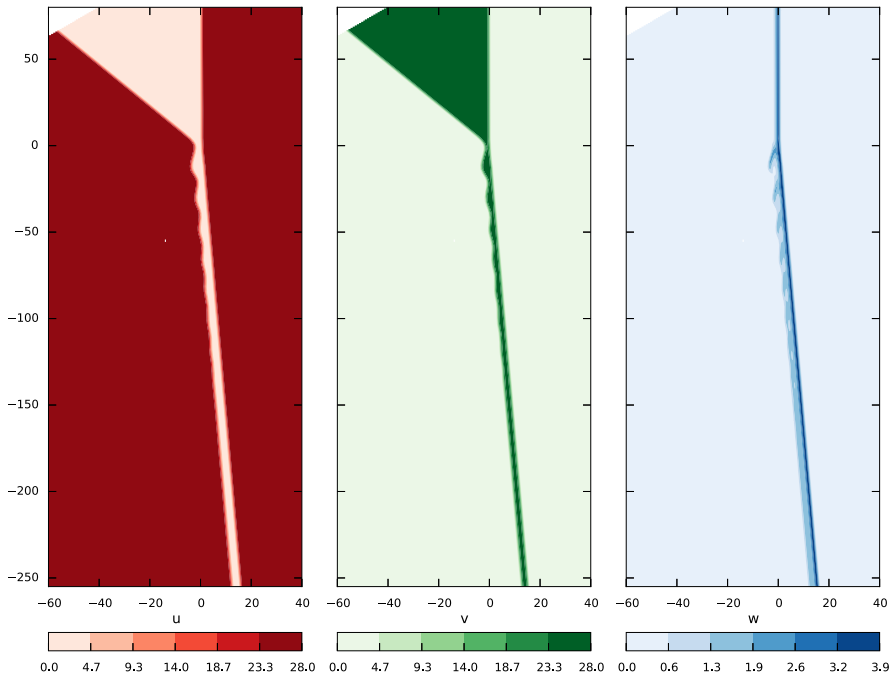


Fig. 25 A zipper-shaped traveling wave arising from the interaction of planar fronts forming an angle $\eta = 0.7$, for $r_3 = 27.12$ and the other parameters specified as in (8), obtained by numerically solving the two-dimensional traveling wave equation associated to (1)

of the two-dimensional traveling wave equation for $\eta = 0.7$ smaller than $\eta_c \approx 1.3$ has been reported in Fig. 25. The computed velocity is $(1.75323, 2.72414)$, while the expected value based on (11)–(12) is $(1.73669, 2.75121)$.

Thus, even when one-dimensional waves interact by reflection, planar waves in two dimensions may merge in a homoclinic front if they do not interact parallelly. This is not completely surprising. As we have seen in Sect. 2.2, the type of interaction in one dimension is closely linked to the speed difference between the fronts: A high speed difference leads to reflection, while speeds which are closer in value produce merging in a homoclinic wave. In two dimensions, the relative speed at which the fronts interact depends on the angle of collision: The larger η is, the smaller this effective speed difference becomes. Thus, even if parallel planar fronts would reflect on collision, considering non-parallel fronts may lead to homoclinic merging. On the other hand, if we consider an angle η sufficiently smaller than the critical angle, we can observe reflection and biwedge-shaped traveling waves also for $r_3 = 27.12$, as can be seen in Fig. 26.

In the previous paragraph, we have explained the imperfect reflection observed in Figs. 4 and 24 as been caused by a reduction in the relative speed of the fronts, which is a purely geometric effect. One could wonder if such a phenomenon is instead due to instability effects. Indeed, for $r_3 = 27.12$ we are near the turning point of the bifurcation diagram for the non-trivial wave and thus near to its unstable branch

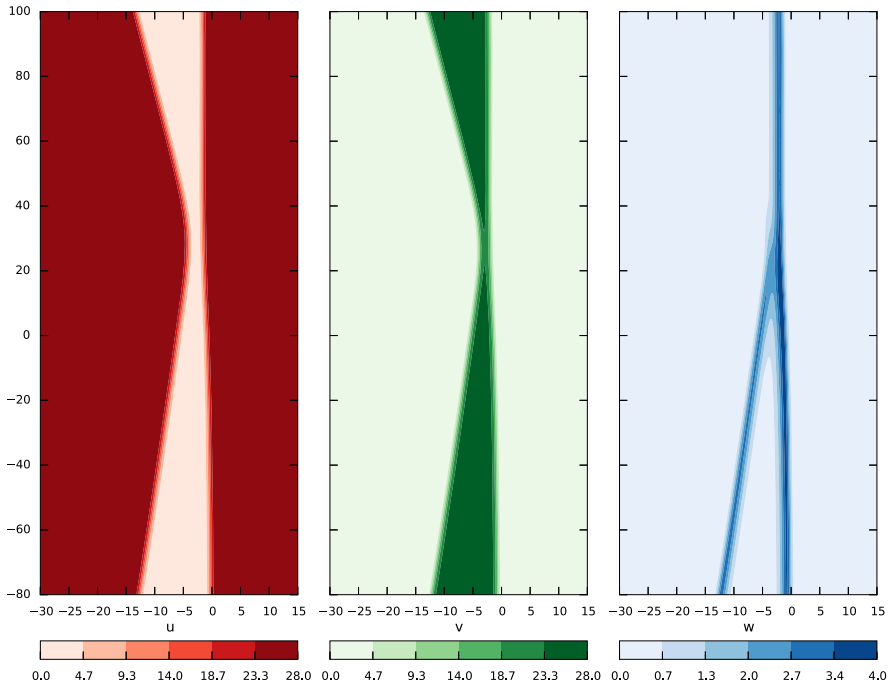


Fig. 26 A biwedge-shaped traveling wave arising from the interaction of planar fronts forming an angle $\eta = 0.15$, for $r_3 = 27.12$ and the other parameters specified as in (8), obtained by numerically solving the two-dimensional traveling wave equation associated to (1)

(see Fig. 7). In order to clear this doubt, we will show that this phenomenon can be observed also when we are far from the unstable branch of the bifurcation curve, thus discarding instability as the most probable mechanism for imperfect reflection. In order to do that, however, we have to use different parameters. We will consider the same parameter values as the ones in [17], i.e., take b_{23} to be a free parameter and set $r_3 = 28$ and the remaining parameters as in (8). The global structure of non-trivial one-dimensional traveling waves as b_{23} varies is qualitatively the same as that of Fig. 7. Similarly, the same basic one-dimensional interactions can be observed as b_{23} changes. For example, for a high speed difference between the two stable waves (e.g., for $b_{23} = 0.4$) reflection can be observed, while for nearly equal speeds (e.g., for $b_{23} = 0.6$) colliding fronts merge in homoclinic ones [17].

Firstly we consider radial-planar interaction for $b_{23} = 0.4$, as shown in Fig. 27. In contrast to Fig. 24, a biwedge-shaped traveling wave appears. The angle between the colliding fronts tends to the critical angle $\eta_c \approx 1.038$ and β has the value predicted in Fig. 26. No imperfect reflection is observed in this case, probably because the speed difference between the fronts is large enough even after considering the effects of non-parallel interaction. Obviously, reflection occurs also for all smaller angles. A biwedged-shaped traveling wave with collision angle $\eta = 0.6$ has been for example reported in Fig. 28. The computed velocity is $(2.04019, 2.13925)$, while the value predicted by (11)–(12) is $(2.02910, 2.13961)$.

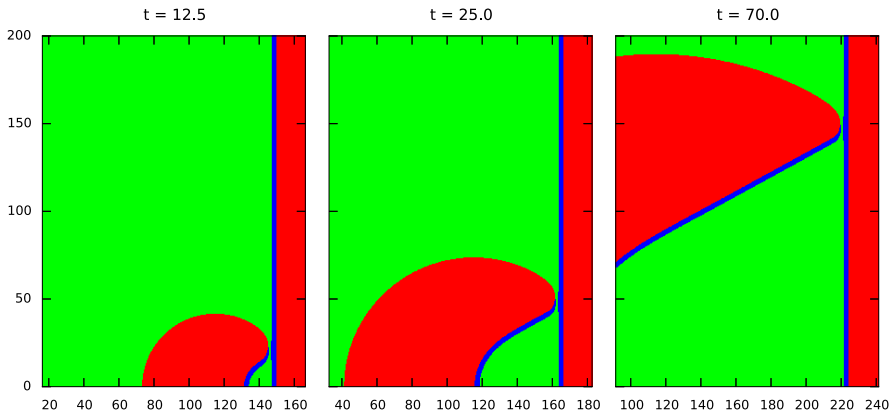


Fig. 27 Interaction of a faster radially expanding trivial front with a slower planar non-trivial front for $r_3 = 28, b_{23} = 0.4$ and the other parameters specified as in (8). Initial conditions are the same as in Fig. 22

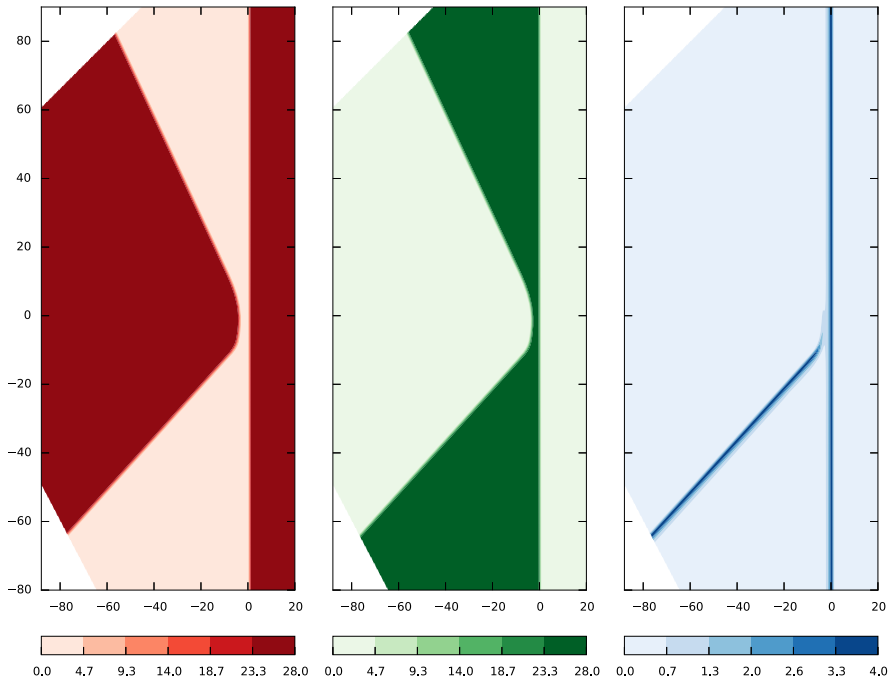


Fig. 28 A biwedge-shaped traveling wave arising from the interaction of planar fronts forming an angle $\eta = 0.6$, for $r_3 = 28, b_{23} = 0.4$ and the other parameters specified as in (8), obtained by numerically solving the two-dimensional traveling wave equation associated to (1)

For values of b_{23} around 0.4 and above the unstable and stable branches of the non-trivial one-dimensional traveling wave are far from each other [17]. Notwithstanding, imperfect reflection can still be observed by tuning the value of b_{23} . If we increase the value of b_{23} starting from 0.4, the difference between the speeds of the trivial

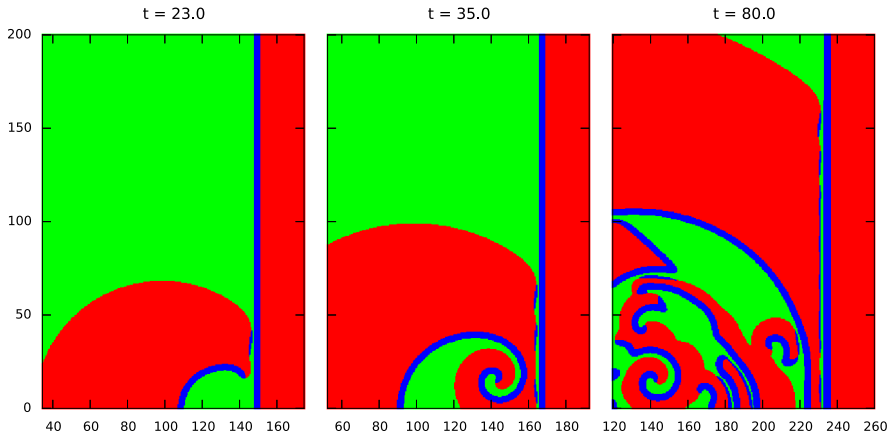


Fig. 29 Interaction of a faster radially expanding trivial front with a slower planar non-trivial front for $r_3 = 28$, $b_{23} = 0.46$ and the other parameters specified as in (8). Initial conditions are the same as in Fig. 22

and non-trivial front gets smaller. If $b_{23} = 0.6$, it becomes small enough to observe homoclinic merging in one dimension (and thus probably in two dimensions too), but for intermediate values we may have a situation similar to Fig. 24, i.e., reflection occurs in one dimension but homoclinic merging may be observed in two dimensions depending on the value of the collision angles. This happens for example for $b_{23} = 0.46$, as shown in Fig. 29. Also in this case we have used AUTO to confirm the existence of a homoclinic traveling wave, which appears to be unstable. The speed of such wave is very close to the non-trivial front speed, which gives $\beta = 0$.

As a last case, we show the results of radial-planar interaction when the non-trivial front is a standing wave. This happens for example when $r_3 = 28$, $b_{23} = 0.029$ and the other parameters are specified as in (8). In this case the one-dimensional behaviour can be classified both as reflection and homoclinic merging, since the reflected front is a standing wave too and the final profile is that of a standing homoclinic wave. Thus, we expect to observe a zipper-shaped traveling wave with $\beta = 0$. Since one of the waves is standing, the critical angle is $\eta_c = \frac{\pi}{2}$: When a radial front and a planar one interact, they will tend to become *perpendicular* to each other. The numerical simulation for this case is reported in Fig. 30. A solution for a smaller angle $\eta = 0.7$ is shown in Fig. 31. Its computed velocity is (1.36121, 3.80935), while the expected one is (1.37048, 3.75444) (we remember that, as before, these are values in the reference frame where the bisector of the topmost wedge is oriented vertically).

5 Interaction of wedge-shaped waves

Numerical simulations of the interaction between wedge-shaped traveling waves are presented in this section. Similarly to the symmetric traveling wave associated to the trivial front, we expect that a symmetric traveling wave with arbitrary angle exists

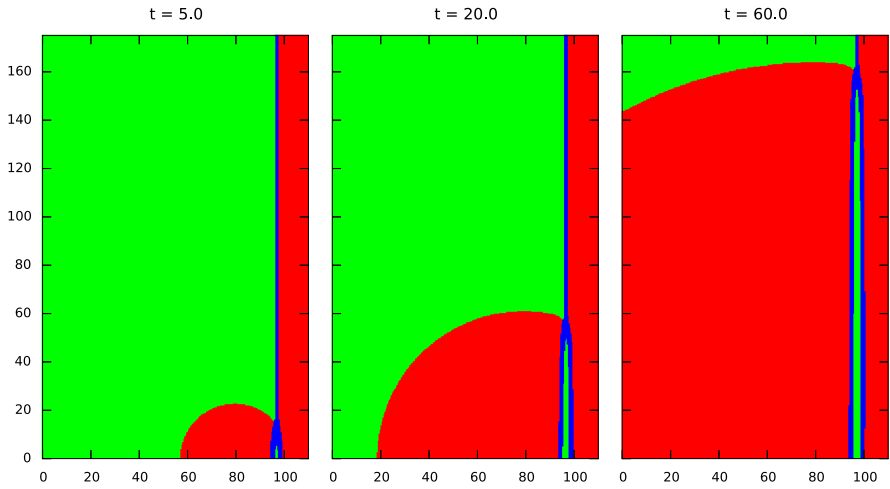


Fig. 30 Interaction of a faster radially expanding trivial front with a standing planar non-trivial front for $r_3 = 28$, $b_{23} = 0.029$ and the other parameters specified as in (8). Initial conditions are the same as in Fig. 22

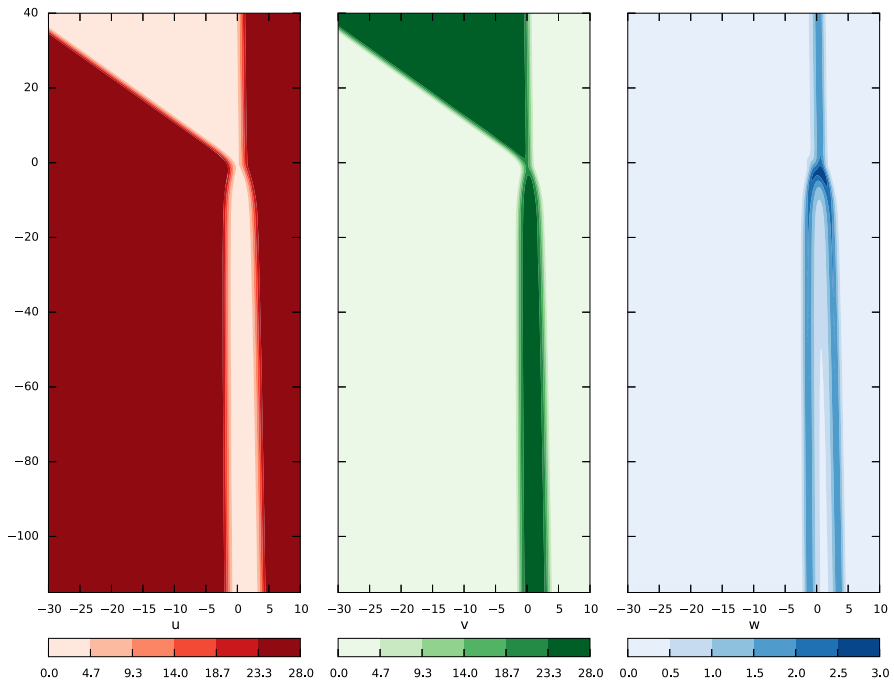


Fig. 31 A zipper-shaped traveling wave arising from the interaction of planar fronts forming an angle $\eta = 0.7$, for $r_3 = 28$, $b_{23} = 0.029$ and the other parameters specified as in (8), obtained by numerically solving the two-dimensional traveling wave equation associated to (1)

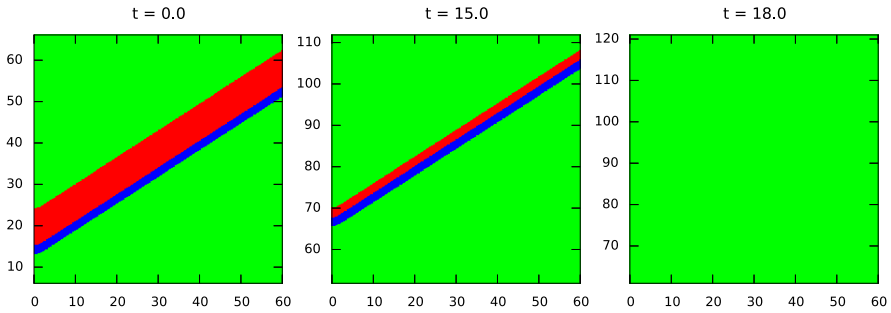


Fig. 32 Interaction of symmetric wedge-shaped non-trivial (*bottom*) and trivial (*top*) fronts for $r_3 = 28.3$, $\eta_b = \eta_t = 2$ and other parameters as in (8). By symmetry with respect to $x = 0$, only half of the domain is shown

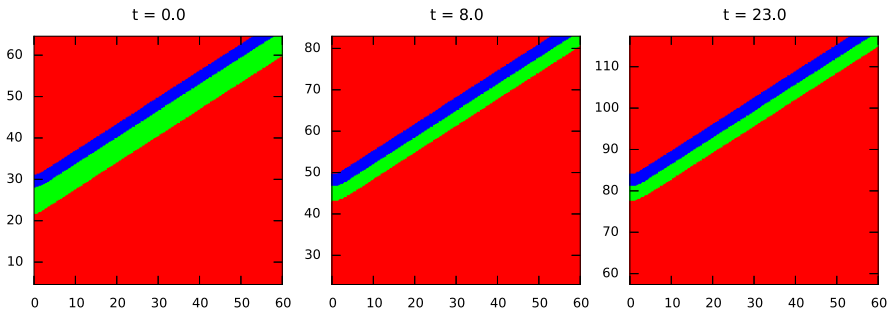


Fig. 33 Interaction of symmetric wedge-shaped trivial (*bottom*) and non-trivial (*top*) fronts for $r_3 = 27.5$, $\eta_b = \eta_t = 2$ and other parameters as in (8). By symmetry with respect to $x = 0$, only half of the domain is shown

also for the non-trivial front. The interaction between trivial and non-trivial symmetric wedges can be thought as a generalization of the interaction between planar fronts. For the sake of simplicity, we consider only the situation in which the bisectors of the two wedges lie on the same line. Let us denote by c_t and c_b the speed of the fronts associated respectively to the top and the bottom wedge and by η_t and η_b their respective angles. By formula (11) the speeds of the two wedges are $c_{wt} := c_t / \sin \eta_t$ and $c_{wb} := c_b / \sin \eta_b$. The wedges will interact if $c_{wt} < c_{wb}$; since we must have $\eta_t \leq \eta_b$ in order for the wedge sides not to intersect, a necessary condition for interaction is $c_t < c_b$. Being this setting completely symmetric with respect to the common bisector of the wedges, numerical simulations will be performed on only half of the domain. A sufficiently large domain (not completely shown in the plots) must be taken in order for the boundary effects not to spread to the region of interest for the length of the simulation.

Firstly we consider the case in which $\eta_t = \eta_b$. Results are reported in Figs. 32, 33, 34 and 35 and, with the exception of the case $r_3 = 27.12$ (Fig. 34), the results are those expected from the one-dimensional behaviour. For $r_3 = 28.3$ we observe annihilation, as shown in Fig. 32. For $r_3 = 27.5$ the wedges merge in the homoclinic symmetric wedge-shaped traveling wave, as shown in Fig. 33. For $r_3 = 28$, $b_{23} = 0.4$ the top

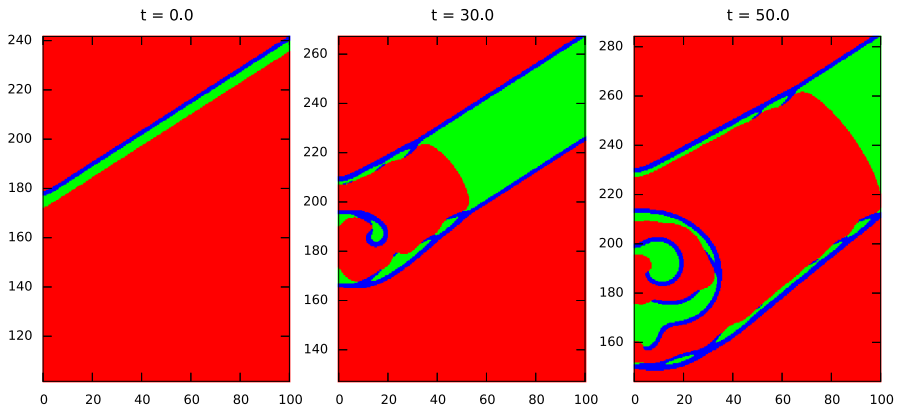


Fig. 34 Interaction of symmetric wedge-shaped trivial (*bottom*) and non-trivial (*top*) fronts for $r_3 = 27.12$, $\eta_b = \eta_t = 2$ and other parameters as in (8). By symmetry with respect to $x = 0$, only half of the domain is shown

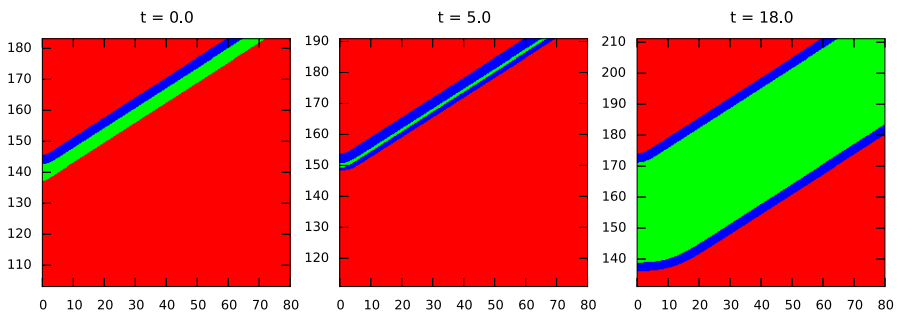


Fig. 35 Interaction of symmetric wedge-shaped trivial (*bottom*) and non-trivial (*top*) fronts for $r_3 = 28$, $b_{23} = 0.4$, $\eta_b = \eta_t = 2$ and other parameters as in (8). By symmetry with respect to $x = 0$, only half of the domain is shown

wedge continues unaffected, while the bottom one is reflected, as shown in Fig. 35; the reflected front will slowly become planar, since there are no symmetric wedge-shaped traveling waves whose velocity is directed outwards. In the case $r_3 = 27.12$ instead, as we already observed when considering interaction of radial and planar fronts, imperfect reflection is observed where the fronts are curved, i.e., near the tips. Far from the tips, where the fronts are parallel, complete reflection is instead achieved. Eventually, two homoclinic fronts moving in opposite directions are created, while in the region between them spiral cores appear and complex patterns are generated, as shown in Fig. 34. It is unclear if the topmost front will converge to a homoclinic symmetric wedge-shaped traveling wave, since the one-dimensional homoclinic wave is unstable in this case.

Next, we consider the case in which $\eta_t < \eta_b$. In this case the wedges do not interact instantly along all their length, but the two points where interaction occur travel along the sides of the top wedge with constant speed. Near these two points we expect to observe patterns similar to those produced by radial-planar interaction, while the shape below them should become similar to the one observed in the $\eta_t = \eta_b$ case. The

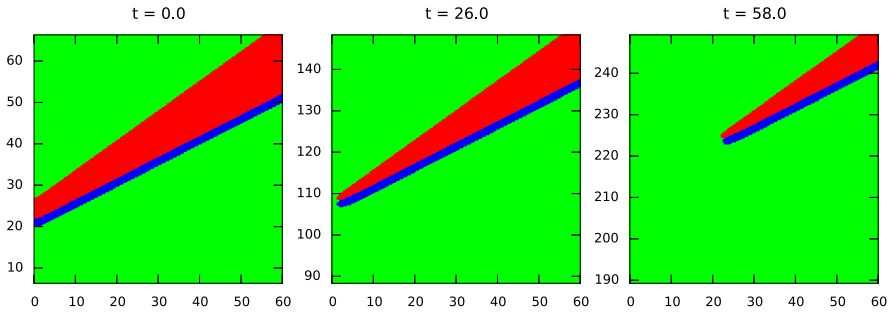


Fig. 36 Interaction of symmetric wedge-shaped non-trivial (*bottom*) and trivial (*top*) fronts for $r_3 = 28.3$, $\eta_b = 2.2$, $\eta_t = 1.9$ and other parameters as in (8). By symmetry with respect to $x = 0$, only half of the domain is shown

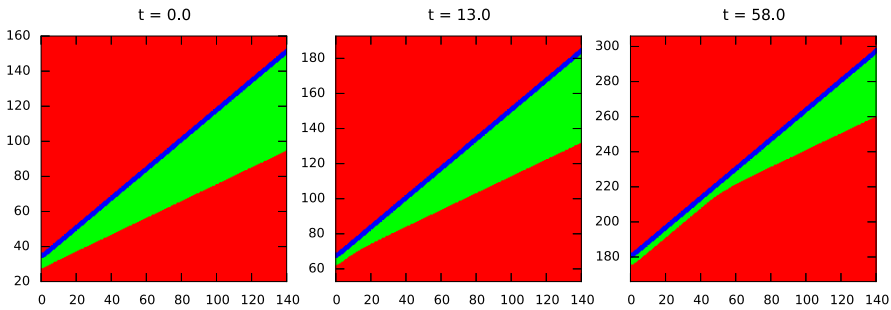


Fig. 37 Interaction of symmetric wedge-shaped trivial (*bottom*) and non-trivial (*top*) fronts for $r_3 = 27.5$, $\eta_b = 2.25$, $\eta_t = 1.75$ and other parameters as in (8). By symmetry with respect to $x = 0$, only half of the domain is shown

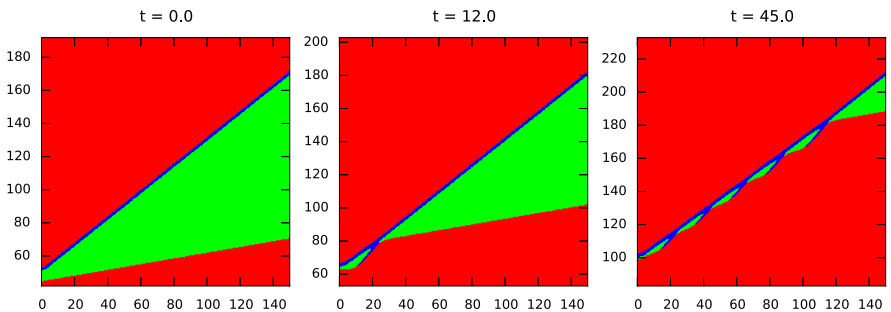


Fig. 38 Interaction of symmetric wedge-shaped trivial (*bottom*) and non-trivial (*top*) fronts for $r_3 = 27.12$, $\eta_b = 2.8$, $\eta_t = 1.8$ and other parameters as in (8). By symmetry with respect to $x = 0$, only half of the domain is shown

numerical simulations confirm this reasoning, as shown in Figs. 36, 37, 38, 39 and 40. Observe that when $r_3 = 27.12$ the behaviour depends on the angle between the sides of different wedges, as happened for the traveling waves of Figs. 25 and 26. If this

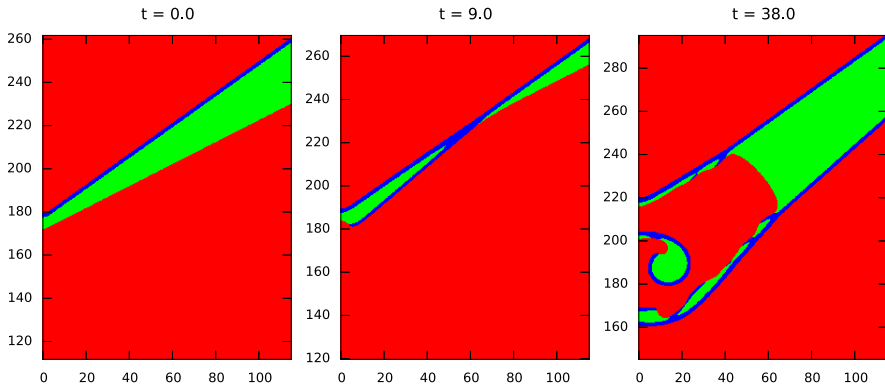


Fig. 39 Interaction of symmetric wedge-shaped trivial (*bottom*) and non-trivial (*top*) fronts for $r_3 = 27.12$, $\eta_b = 2.2$, $\eta_t = 1.9$ and other parameters as in (8). By symmetry with respect to $x = 0$, only half of the domain is shown

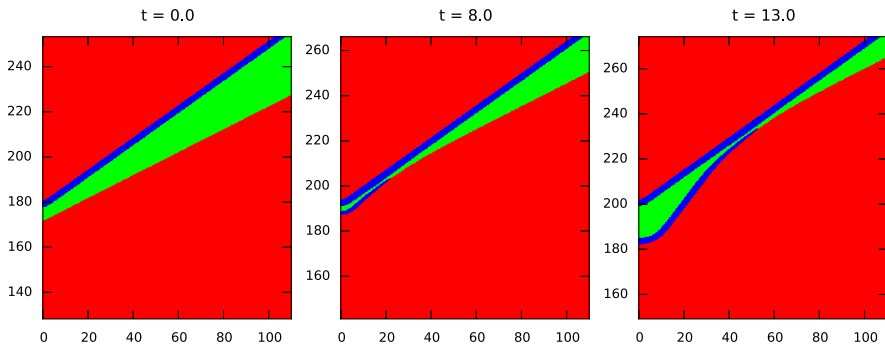


Fig. 40 Interaction of symmetric wedge-shaped trivial (*bottom*) and non-trivial (*top*) fronts for $r_3 = 28$, $b_{23} = 0.4$, $\eta_b = 2.2$, $\eta_t = 1.9$ and other parameters as in (8). By symmetry with respect to $x = 0$, only half of the domain is shown

angle is large (Fig. 38), the fronts merge into a homoclinic one, while if it is smaller (Fig. 39), the fronts reflect on collision.

As a final example of possible interaction between wedge-shaped traveling waves, we consider the collision of two asymmetric wedges. As before, we assume symmetry, which in particular means that the angle of the two wedges is the same. This situation is again described by η_t and η_b , the angles formed respectively between the two topmost and the two bottommost sides of the wedges. We have that the wedge angle is $\eta = (\eta_b - \eta_t)/2$. If the angles are chosen appropriately, the two wedges will move toward each other and collide. After collision we may expect two symmetric wedge-shaped fronts to be formed from respectively the top and the bottom sides of the original two wedges. Since the condition for having collision between the asymmetric wedges is equivalent to $c_{wt} > c_{wb}$, we may expect these two new symmetric wedges to separate and the gap between them to become larger as time progresses. This is confirmed by numerical simulation, as shown in Fig. 41.

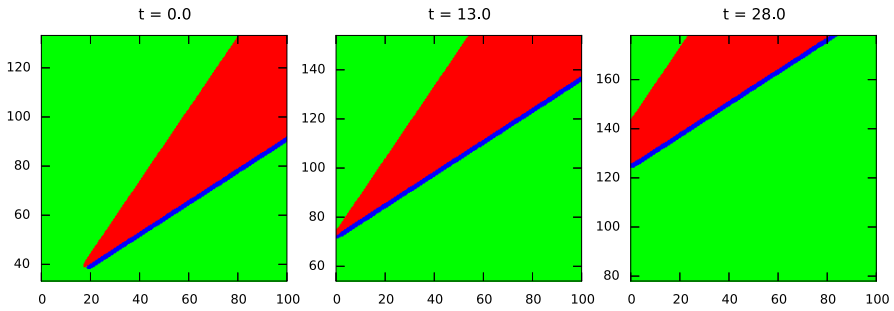


Fig. 41 Interaction of two asymmetric wedge-shaped fronts for $r_3 = 28.3$, $\eta_b = 2$, $\eta_l = 1.2$ and other parameters as in (8). By symmetry with respect to $x = 0$, only half of the domain is shown

6 Conclusions

In this paper we have presented several types of two-dimensional traveling waves, all sharing the property of being asymptotically planar: They consist of several fronts which converge and interact in a single point, but tend in shape to planar fronts at spatial infinities. Many properties of these waves, such as their velocity and the conditions for their existence, can be derived heuristically just by considering them as a bundle of independently propagating planar fronts, neglecting the behaviour near the interaction point.

The number of such two-dimensional waves we can build is limited by the number of different (stable) planar fronts and by the number of possible interaction behaviour between such fronts. Simpler systems such as the Allen–Cahn equation or the two-species competition-diffusion system have already been shown to exhibit wedge-shaped traveling waves, albeit only of the symmetric type. This is the only possible type of wave in such systems, since they admit only one stable planar wave which can only interact destructively with itself. In a three-species competition-diffusion system instead, the situation is drastically different: The possibility of competitor-mediated coexistence is reflected in the existence of two different stable fronts and by controlling the strength of the exotic species, it is possible to change the way these two waves interact. These two facts give rise to all the novel traveling wave shapes presented in this paper. On the other hand, we think the additional complexity of such a three-species system makes obtaining an existence proof for these waves more difficult. For example, the proofs presented in [21, 22] are not straightforward to generalize to our case since they rely on the comparison principle, not applicable in our case. Moreover, other than the existence problem, the stability of the two-dimensional traveling waves presented in this paper should be further investigated.

We think it should be possible to construct even more complicated traveling waves by using only planar fronts. Take for example $r_3 = 28$, $b_{23} = 0.4$ and the other parameters as in (8). Consider biwedge-like initial conditions where the top angle is greater than η_c . Then, the collision angle naturally decreases to the critical one and in the lower part of the domain several triangular patterns are generated, as shown in Fig. 42a. In each of these triangles, two of the vertices correspond to reflection events, while the other one is the tip of a symmetric-wedge, given by the annihilation

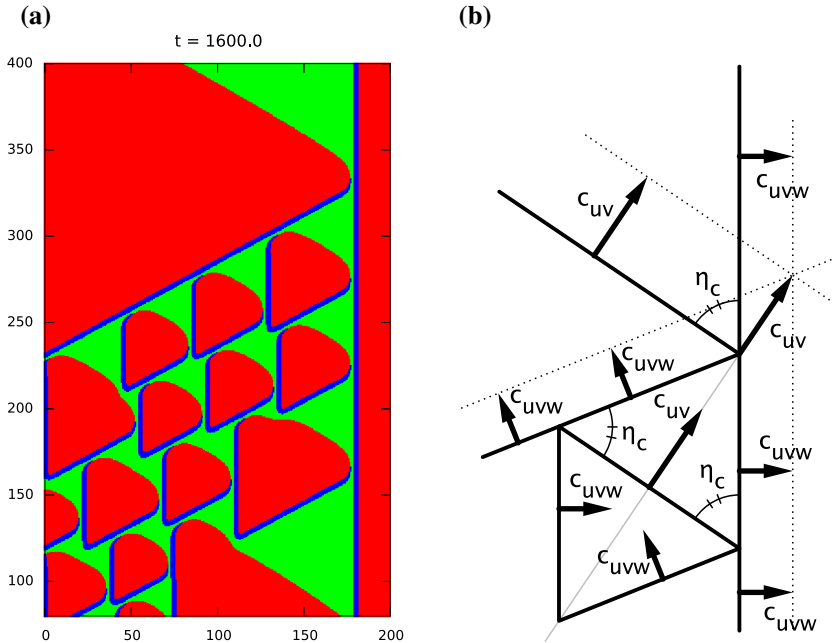


Fig. 42 A hypothetical composite wave when reflection occurs between the fronts. **a** Triangular patterns appearing for biwedge-like initial conditions for $r_3 = 28$, $b_{23} = 0.4$ and the other parameters specified as in (8). **b** Prediction about the geometrical structure of a composite traveling wave. Note that this is only possible if the topmost angle is the critical one

of two non-trivial fronts. If, as in this case, collision between the main fronts occurs at the critical angle, any such triangle should move with the same velocity as the full traveling wave, as shown in Fig. 42b. However, because of interactions between the triangles and possibly because of their small size, this pattern is not stationary and triangles merge and break up. Further investigation is needed to ascertain whether such composite traveling waves actually exist or not.

Appendix A: Proof of the velocity formula for asymptotically planar traveling waves

We will now give a more formal proof for the relation $\mathbf{c} - \mathbf{c}_p \perp \mathbf{c}_p$, where \mathbf{c} is the velocity of a two-dimensional traveling wave whose shape in one asymptotic direction tends to that of a planar front with velocity \mathbf{c}_p . This relation was used in Sect. 3.2 to derive the formulas (11)–(12) for the velocity of asymptotically planar traveling waves, of which wedge-shaped traveling waves are an example.

Theorem Consider the following equation in the variables $\mathbf{u} : \mathbb{R}^n \rightarrow \mathbb{R}^m$ and $\mathbf{c} \in \mathbb{R}^n$

$$\mathbf{D}\Delta\mathbf{u} + \nabla\mathbf{u}\mathbf{c} + \mathbf{f}(\mathbf{u}) = \mathbf{0} \text{ in } \mathbb{R}^n, \tag{15}$$

where $\mathbf{D} \in \mathbb{R}^{m \times m}$ is a positive diagonal matrix, $\nabla \mathbf{u} : \mathbb{R}^n \rightarrow \mathbb{R}^{m \times n}$ is the Jacobian of \mathbf{u} and $\mathbf{f} : \mathbb{R}^m \rightarrow \mathbb{R}^m$.

Suppose that:

1. (\mathbf{u}, \mathbf{c}) and $(\mathbf{u}_p, \mathbf{c}_p)$ are solutions of (15) such that $\mathbf{c}_p \neq 0$ and $\mathbf{u}, \mathbf{u}_p \in \mathcal{C}^2(\mathbb{R}^n, \mathbb{R}^m)$;
2. $\mathbf{f} : \mathbb{R}^m \rightarrow \mathbb{R}^m$ is Lipschitz continuous on the set $\mathbf{u}(\mathbb{R}^n) \cup \mathbf{u}_p(\mathbb{R}^n)$;
3. for every $\varepsilon > 0$ there exists $\Omega_\varepsilon \subset \mathbb{R}^n$ bounded such that

$$\|(\mathbf{u} - \mathbf{u}_p)|_{\Omega_\varepsilon}\|_{\mathcal{C}^2(\Omega_\varepsilon, \mathbb{R}^m)} < \varepsilon. \tag{16}$$

4. there exists a constant $\delta > 0$ such that for every $\varepsilon > 0$ there exists $\alpha_\varepsilon \in \mathbb{R}^m$, $\mathbf{n}_\varepsilon \in \mathbb{R}^n$ and $x_\varepsilon \in \Omega_\varepsilon$ satisfying

$$\nabla \mathbf{u}_p(x_\varepsilon) = \alpha_\varepsilon \mathbf{n}_\varepsilon^t, \tag{17}$$

$$|\mathbf{n}_\varepsilon| = 1, \tag{18}$$

$$|\alpha_\varepsilon| > \delta, \tag{19}$$

where $|\cdot|$ is the Euclidean norm.

Then, there exists a sequence $\varepsilon_k \rightarrow 0$ and $\mathbf{n} \in \mathbb{R}^n$ such that $\mathbf{n}_{\varepsilon_k} \rightarrow \mathbf{n}$ and $|\mathbf{n}| = 1$. Moreover, we have that $\mathbf{c} - \mathbf{c}_p \perp \mathbf{n}$.

Proof By (18) we have that $\{\mathbf{n}_\varepsilon\}_{\varepsilon > 0}$ is contained in the compact boundary of the unit ball of \mathbb{R}^n . Thus existence of a limit vector $\mathbf{n} \in \mathbb{R}^n$ such that $|\mathbf{n}| = 1$ is immediately established.

Subtracting the equations obtained from (15) by substitution with (\mathbf{u}, \mathbf{c}) and $(\mathbf{u}_p, \mathbf{c}_p)$ respectively, we get

$$\mathbf{D}(\Delta \mathbf{u} - \Delta \mathbf{u}_p) + \nabla \mathbf{u} \mathbf{c} - \nabla \mathbf{u}_p \mathbf{c}_p + \mathbf{f}(\mathbf{u}) - \mathbf{f}(\mathbf{u}_p) = \mathbf{0} \text{ in } \mathbb{R}^n.$$

If we add $\nabla \mathbf{u}_p \mathbf{c}$ to both sides, we obtain after rearrangement

$$\nabla \mathbf{u}_p(\mathbf{c} - \mathbf{c}_p) = \mathbf{D}(\Delta \mathbf{u}_p - \Delta \mathbf{u}) + (\nabla \mathbf{u}_p - \nabla \mathbf{u})\mathbf{c} + \mathbf{f}(\mathbf{u}_p) - \mathbf{f}(\mathbf{u}) \text{ in } \mathbb{R}^n.$$

Now fix $\varepsilon > 0$ and consider only $x \in \Omega_\varepsilon$. We take the Euclidean norm on both sides. By Lipschitz continuity of \mathbf{f} and (16), we get

$$|\nabla \mathbf{u}_p(\mathbf{c} - \mathbf{c}_p)| < K\varepsilon \text{ in } \Omega_\varepsilon \tag{20}$$

for $K = \text{tr } \mathbf{D} + K'|\mathbf{c}| + L$, where tr is the matrix trace operator, K' is due to the conversion from the operatorial norm of $\nabla \mathbf{u}_p - \nabla \mathbf{u}$ to its maximum norm and L is the Lipschitz constant for \mathbf{f} .

Evaluating (20) at x_ε and using (17) we get,

$$|\alpha_\varepsilon \mathbf{n}_\varepsilon^t(\mathbf{c} - \mathbf{c}_p)| < K\varepsilon.$$

By applying the lower bound on $|\alpha_\varepsilon|$ given in (19), we obtain

$$K\varepsilon > |\alpha_\varepsilon| |\mathbf{n}_\varepsilon^t (\mathbf{c} - \mathbf{c}_p)| > \delta |\mathbf{n}_\varepsilon^t (\mathbf{c} - \mathbf{c}_p)|.$$

Since this inequality holds for every $\varepsilon > 0$, by considering it on the sequence $\{\varepsilon_k\}_k$ and taking the limit we obtain $\mathbf{n}^t (\mathbf{c} - \mathbf{c}_p) = 0$, which is equivalent to saying that $\mathbf{c} - \mathbf{c}_p \perp \mathbf{n}$. □

Corollary *In the setting of the above Theorem, consider the following additional hypothesis: \mathbf{u}_p is a planar front and $\mathbf{c}_p = |\mathbf{c}_p| \mathbf{n}$, where \mathbf{n} is the unit vector normal to the front. Then,*

$$\mathbf{c} - \mathbf{c}_p \perp \mathbf{c}_p. \tag{21}$$

Proof Note that we may denote the normal to the front with the symbol \mathbf{n} without any abuse of notation. Indeed, we have that $\mathbf{n}_\varepsilon = \mathbf{n}$ for all $\varepsilon > 0$ due to the front being planar. By the above Theorem and by our choice of \mathbf{c}_p we get

$$\mathbf{n}^t (\mathbf{c} - \mathbf{c}_p) = \frac{\mathbf{c}_p^t}{|\mathbf{c}_p|} (\mathbf{c} - \mathbf{c}_p) = 0,$$

from which (21) immediately follows. □

Remark The lower bound on the norm of $\nabla \mathbf{u}_p(x_\varepsilon)$ is essential. Otherwise, we could take any two traveling wave solutions sharing one asymptotic equilibrium state and the above Theorem would apply. For example, it could be applied to two different orientations of the same planar front, which is clearly impossible.

Appendix B: Numerical solution of the traveling wave equation in two dimensions

As stated at the beginning of Sect. 3.3, we need to find a numerical method appropriate to the computation of traveling wave solutions. We are interested both in solving the stationary problem given by the traveling equation (14) and the time-evolution problem given by (1). The main difficulty lies in the fact that the domain in which these problems are posed is the whole space (in our case \mathbb{R}^2), whereas numerical methods are in general limited to bounded domains. However, in the case of traveling wave solutions the asymptotic behavior at spatial infinity is given. This means that a bounded domain Ω is sufficient if it is large enough to cover the area where the solution differs substantially from the asymptotic behaviour, which is where the non-trivial and interesting features of the wave lie. The faster the solution converges to the asymptotic state for $|x| \rightarrow \infty$, the smaller the domain Ω can be taken. Apart from the choice of Ω , we must determine which boundary conditions the numerical solution should satisfy on $\partial\Omega$. These conditions should be chosen such that also the true traveling wave solution satisfies them, at least approximately.

As a simple and well-known example, consider the traveling wave equation (14) in one spatial dimension. In order to specify the asymptotic behaviour, it is sufficient

to set the two limit values of the solution for $x \rightarrow \pm\infty$, as it is done for example in the problem (5)–(6). In many cases, by choosing $\Omega = (-L, L)$ with $L > 0$ large enough, we can capture all the most relevant information about the one-dimensional traveling wave, since such information is often concentrated around the wave front. Outside Ω , the solution is approximately equal to the asymptotic equilibrium states. This means that the exact traveling wave not only approximately satisfies a couple of Dirichlet boundary conditions on $\partial\Omega = \{-L, L\}$, but it is also approximately compatible with Neumann zero-flux boundary conditions, since its derivatives must tend to 0 for $x \rightarrow \pm\infty$.

Now consider the two-dimensional case. The asymptotic behaviour consists in two or more fronts which propagate independently. While in \mathbb{R} the possible choices for the bounded domain Ω are essentially intervals, in \mathbb{R}^2 a great variety of shapes is possible in theory. As for the boundary conditions, Dirichlet type conditions can be used for any large enough choice of Ω , since the asymptotic behaviour is known. A possible drawback is that the asymptotic state must be computed beforehand. In our case, since the traveling wave is asymptotically planar, this computation can be reduced to a one-dimensional traveling wave equation for each front. While such simplification helps in term of computational time, using different discretizations for the one- and two-dimensional problems may introduce an additional source of error. Moreover, when studying the interaction of different waves, the value at the boundary changes with time, making Dirichlet conditions inapplicable.

In order to derive boundary conditions other than Dirichlet, the asymptotic behaviour of the gradient of the traveling wave should be studied. Far from all the fronts the solution tends to one of the equilibrium states and thus its gradient tends to $\mathbf{0}$. On the other hand, for a point $x \in \mathbb{R}^2$ in the vicinity of a front the solution asymptotically satisfies

$$\frac{\partial \mathbf{u}}{\partial v_f(x)}(x) = \mathbf{0}, \quad (22)$$

where $v_f(x)$ is the unit vector perpendicular to the asymptotic direction of propagation of the front nearest to x . Note that points for which the gradient is approximately $\mathbf{0}$ satisfy also condition (22). Then, we may take (22) as the boundary condition for the whole $\partial\Omega$. This is a case of an *oblique boundary condition* (see for example [16]). This choice reduces to the Neumann zero-flux boundary conditions in the case $v_f(x) = v(x)$ for every $x \in \partial\Omega$, where $v(x)$ is the unit vector normal to $\partial\Omega$ at x . This is also true if we let the shape of $\partial\Omega$ violate $v_f = v$ far from all the fronts, since the gradient is approximately $\mathbf{0}$ there: this fact allows $\partial\Omega$ to be a closed curve. In practice, this means that, if we want to use zero-flux boundary conditions, Ω must be a polygon whose edges are normal to the front they intersect.

Thus, in the case of wedge-shaped traveling waves and rectangular domains as those used in Figs. 3, 4, 5 and 6, zero-flux boundary conditions do not yield the correct result: all fronts are forced to gradually become perpendicular to the boundary, which results in the sides of the wedge becoming parallel and eventually colliding, leading to the disappearance of the wedge feature. While a rectangular domain may be employed by implementing the oblique boundary conditions in the numerical method, we preferred

to use the simpler zero-flux conditions by adopting a polygonal domain whose edges are perpendicular to the fronts. For example, in our computations for wedge-shaped traveling waves we use a pentagonal domain with the two topmost edges normal to the wedge sides, the base orthogonal to the wedge bisector and the remaining two edges parallel to the fronts. More complicated domains are needed for zipper- and biwedge-shaped traveling waves, as can be seen for example in Fig. 28. In order to deal with non-rectangular domains, we employ a continuous piecewise-linear finite element discretization using the software FreeFem++ [10]. Adaptive mesh refinement is also adopted in order to reduce the size of the discretized system.

Other well-known difficulties concerning the traveling equation (14) are that \mathbf{c} is an unknown to be solved for, which leads to a non-square linear system in the discretized problem, and the solution is no longer unique, since the traveling wave equation is invariant with respect to translation. These two problems can be solved at the same time by specifying additional constraints. In particular, we enforce *integral phase conditions* [3], which are also used by the popular continuation package AUTO [6] in the context of numerical computation of orbits of ODEs [5] (in one dimension traveling waves are essentially homoclinic orbits of the ODE associated to the traveling wave equation). Since in our case the position of two planar fronts uniquely determines the position of the full traveling wave, we can apply two one-dimensional phase conditions to two edges of $\partial\Omega$ instead of one two-dimensional phase condition to the whole Ω .

We are also interested in solving the time-evolution problem (1), especially in order to obtain an approximate solution to bootstrap the Newton solver for the associated two-dimensional traveling wave equation. Here the difficulty is that traveling waves leave the computational domain Ω in a finite time. As usual in such cases, we employ a moving reference frame, which is equivalent to consider the time-evolution problem associated to the traveling wave equation (14). Since the velocity of the traveling wave is not known a priori, we have to adapt the frame velocity to the current velocity of the wave in order to keep it centered inside Ω . To this purpose, we periodically track the points where two of the planar fronts intersect the boundary and use their velocities to compute the velocity of the whole wave by applying formulas (11)–(12). This expedient is adequate for our needs, though we remark that more elegant, but more complicated, methods may be employed. For example, the frame velocity can be considered as a variable evolving with time and by imposing the phase condition at all times a partial differential algebraic equation (PDAE) can be obtained. Using the method of lines this PDAE can be reduced to a differential algebraic equation (DAE) and solved numerically. This approach, which is called *freezing* the traveling wave, has been proposed independently in [2] and [25]. An introduction to the theory and numerical methods for DAEs can be found in [24] instead.

References

1. Adamson, M.W., Morozov, A.Y.: Revising the role of species mobility in maintaining biodiversity in communities with cyclic competition. *Bull. Math. Biol.* **74**(9), 2004–2031 (2012). doi:[10.1007/s11538-012-9743-z](https://doi.org/10.1007/s11538-012-9743-z)
2. Beyn, W.J., Thümmler, V.: Freezing solutions of equivariant evolution equations. *SIAM J. Appl. Dyn. Syst.* **3**(2), 85–116 (2004). doi:[10.1137/030600515](https://doi.org/10.1137/030600515)

3. Beyn, W.J., Thümmler, V.: Phase conditions, symmetries and pde continuation. In: Krauskopf, B., Osinga, H., Galán-Vioque, J. (eds.) *Numerical Continuation Methods for Dynamical Systems*, pp. 301–330. Springer Netherlands (2007). doi:[10.1007/978-1-4020-6356-5_10](https://doi.org/10.1007/978-1-4020-6356-5_10)
4. Conway, E., Hoff, D., Smoller, J.: Large time behavior of solutions of systems of nonlinear reaction-diffusion equations. *SIAM J. Appl. Math.* **35**(1), 1–16 (1976). doi:[10.1137/0135001](https://doi.org/10.1137/0135001)
5. Doedel, E.J.: AUTO: a program for the automatic bifurcation analysis of autonomous systems. *Congr. Numer.* **30**, 265–284 (1981)
6. Doedel, E.J., Oldeman, B.E., Champneys, A.R., Dercole, F., Fairgrieve, T.F., Kuznetsov, Y., Paffenroth, R.C., Sandstede, B., Wang, X.J., Zhang, C.H.: AUTO-07p: continuation and bifurcation software for ordinary differential equations (2012). <http://sourceforge.net/projects/auto-07p/>
7. Ei, S., Ikota, R., Mimura, M.: Segregating partition problem in competition-diffusion systems. *Interfaces Free Bound* **1**(1), 57–80 (1999). doi:[10.4171/IFB/4](https://doi.org/10.4171/IFB/4)
8. Ei, S., Yanagida, E.: Dynamics of interfaces in competition-diffusion systems. *SIAM J. Appl. Math.* **54**(5), 1355–1373 (1994). doi:[10.1137/S0036139993247343](https://doi.org/10.1137/S0036139993247343)
9. Gause, G.F.: *The Struggle for Existence*. The Williams & Wilkins Company, Baltimore (1934)
10. Hecht, F.: New development in FreeFem++. *J. Numer. Math.* **20**(3–4), 251–265 (2012)
11. Hirsch, M.W.: *Differential equations and convergence almost everywhere of strongly monotone semiflows*. Tech. rep., University of California, Berkeley (1982)
12. Hofbauer, J., Sigmund, K.: *Evolutionary Games and Population Dynamics*. Cambridge University Press, Cambridge (1998)
13. Kan-On, Y.: Fisher wave fronts for the Lotka–Volterra competition model with diffusion. *Nonlinear Anal. Theory Methods Appl.* **28**(1), 145–164 (1997). doi:[10.1016/0362-546X\(95\)00142-1](https://doi.org/10.1016/0362-546X(95)00142-1)
14. Kan-On, Y., Fang, Q.: Stability of monotone travelling waves for competition-diffusion equations. *Japan J. Ind. Appl. Math.* **13**(2), 343–349 (1996). doi:[10.1007/BF03167252](https://doi.org/10.1007/BF03167252)
15. Kishimoto, K., Weinberger, H.F.: The spatial homogeneity of stable equilibria of some reaction-diffusion systems on convex domains. *J. Differ. Equ.* **58**(1), 15–21 (1985). doi:[10.1016/0022-0396\(85\)90020-8](https://doi.org/10.1016/0022-0396(85)90020-8)
16. Lieberman, G.M.: *Oblique Derivative Problems for Elliptic Equations*. World Scientific, Singapore (2013)
17. Mimura, M., Tohma, M.: Dynamic coexistence in a three-species competition diffusion system. *Ecol. Complex.* **21**, 215–232 (2015). doi:[10.1016/j.ecocom.2014.05.004](https://doi.org/10.1016/j.ecocom.2014.05.004)
18. Morita, Y., Tachibana, K.: An entire solution to the Lotka–Volterra competition-diffusion equations. *SIAM J. Math. Anal.* **40**(6), 2217–2240 (2009). doi:[10.1137/080723715](https://doi.org/10.1137/080723715)
19. Morris, S.: Belousov Zhabotinsky reaction $8\times$ normal speed. <http://www.youtube.com/watch?v=3JAqrRnKFHo>. Accessed 24 June 2015
20. Murray, J.D.: *Mathematical Biology: I. An Introduction*. Springer, New York (2002)
21. Ni, W.M., Taniguchi, M.: Traveling fronts of pyramidal shapes in competition-diffusion systems. *Netw. Heterog. Media* **8**(1), 379–395 (2013). doi:[10.3934/nhm.2013.8.379](https://doi.org/10.3934/nhm.2013.8.379)
22. Ninomiya, H., Taniguchi, M.: Existence and global stability of traveling curved fronts in the Allen–Cahn equations. *J. Differ. Equ.* **213**(1), 204–233 (2005). doi:[10.1016/j.jde.2004.06.011](https://doi.org/10.1016/j.jde.2004.06.011)
23. Petrovskii, S., Kawasaki, K., Takasu, F., Shigesada, N.: Diffusive waves, dynamical stabilization and spatio-temporal chaos in a community of three competitive species. *Japan J. Ind. Appl. Math.* **18**(2), 459–481 (2001). doi:[10.1007/BF03168586](https://doi.org/10.1007/BF03168586)
24. Rabier, P.J., Rheinboldt, W.C.: Theoretical and numerical analysis of differential-algebraic equations. In: *Solution of Equations in \mathbb{R}^n* (Part 4), *Techniques of Scientific Computing* (Part 4), *Numerical Methods for Fluids* (Part 2), *Handbook of Numerical Analysis*, vol. 8, pp. 183–540. Elsevier, Amsterdam (2002). doi:[10.1016/S1570-8659\(02\)08004-3](https://doi.org/10.1016/S1570-8659(02)08004-3)
25. Rowley, C.W., Kevrekidis, I.G., Marsden, J.E., Lust, K.: Reduction and reconstruction for self-similar dynamical systems. *Nonlinearity* **16**(4), 1257–1275 (2003). doi:[10.1088/0951-7715/16/4/304](https://doi.org/10.1088/0951-7715/16/4/304)
26. Tohma, M.: *Model-aided understanding of competitor-mediated coexistence*. Ph.D. thesis, Graduate School of Advanced Mathematical Sciences, Meiji University (2013)
27. Zeeman, M.L.: Hopf bifurcations in competitive three-dimensional Lotka–Volterra systems. *Dyn. Stab. Syst.* **8**(3), 189–216 (1993). doi:[10.1080/02681119308806158](https://doi.org/10.1080/02681119308806158)